Distinguishing between old and modern permafrost sources in the Northeast Siberian land-shelf system with compound-specific δ^2H analysis

Jorien E. Vonk[1], Tommaso Tesi[2,3], Lisa Bröder[2,4], Henry Holmstrand[2,4], Gustaf Hugelius[4,5], August Andersson[2,4], Oleg Dudarev[6,7], Igor Semiletov[6,7,8], Örjan Gustafsson[2,4]

[1] Department of Earth Sciences, VU University, The Netherlands
[2] Department of Environmental Science and Analytical Chemistry, Stockholm University, Sweden
[3] ISMAR Institute of Marine Sciences, Bologna, Italy
[4] Bolin Centre for Climate Research, Stockholm University, Sweden
[5] Department of Physical Geography, Stockholm University, Sweden
[6] Pacific Oceanological Institute FEBRAS, Vladivostok, Russia
[7] Tomsk Polytechnic University, Tomsk, Russia
[8] University of Alaska Fairbanks, Fairbanks, USA

Correspondence to: Jorien Vonk (j.e.vonk@vu.nl)

Keywords: deuterium isotopes, yedoma, ice complex deposit, n-alkanoic acids, n-alkanes, organic matter, stable carbon isotopes, radiocarbon, Siberian Arctic, sediments, permafrost thaw

Abstract

Pleistocene ice complex permafrost deposits contain roughly a quarter of the organic carbon (OC) stored in permafrost terrain. When permafrost thaws, its OC is remobilized into the (aquatic) environment where it is available for degradation, transport or burial. Aquatic or coastal environments contain sedimentary reservoirs that can serve as archives of past climatic change. As permafrost thaw is increasing throughout the Arctic, these reservoirs are important locations to assess the fate of remobilized permafrost OC.

We here present compound-specific deuterium (δ^2H) analysis on leaf waxes as a tool to distinguish between OC released from thawing Pleistocene permafrost (Ice Complex Deposits; ICD) and from thawing Holocene permafrost (from near-surface soils). Bulk geochemistry (%OC, $\delta^{13}C$, %total nitrogen; TN) was analyzed as well as the concentrations and δ^2H signatures of long-chain *n*-alkanes (C_{21} to C_{33}) and mid/long-chain *n*-alkanoic acids (C_{16} to C_{30}) extracted from both ICD-PF samples (n=9) and modern vegetation/O-horizon (Topsoil-PF) samples (n=9) from across the northeast Siberian Arctic.

Results show that these Topsoil-PF samples have higher %OC, higher OC/TN values, and more depleted $\delta^{13}C$-OC values than ICD-PF samples, suggesting that these former samples trace a fresher soil and/or vegetation source. Whereas the two investigated sources differ on the bulk geochemical level, they are, however, virtually indistinguishable when using leaf wax concentrations and ratios.

However, on the molecular-isotope level, leaf wax biomarker δ^2H values are statistically different between Topsoil-PF and ICD-PF. For example, the mean δ^2H value of C_{29} *n*-alkane was -246±13‰ (mean±stdev) for Topsoil-PF and -280±12‰ for ICD-PF. With a dynamic isotopic range (difference between two sources) of 34 to 50‰, the isotopic fingerprints of individual, abundant, biomarker molecules from leaf waxes can thus serve as end-members to distinguish between these two sources. We tested this molecular δ^2H tracer along with another source-distinguishing approach, dual-carbon ($\delta^{13}C$-$\Delta^{14}C$) isotope composition of bulk OC, for a surface sediment transect in the Laptev Sea. Results show that general offshore patterns along the shelf-slope transect are similar, but the source apportionment between the approaches vary, which may highlight the advantages of either. This study indicates that the application of δ^2H leaf wax values has potential to serve as a complementary quantitative measure of the source and differential fate of OC thawed out from different permafrost compartments.

1 Introduction

Climate warming is causing permafrost soils to thaw, exposing its organic matter (OM) to decomposition (e.g., Schuur et al., 2015; Zimov et al., 1993; Semiletov et al., 2012). Thaw will increase the hydrological connectivity of landscapes and will cause release of OM into the aquatic environment (Walvoord et al., 2012; Vonk et al., 2015; Anderson et al., 2011). Here, the OM can continue to decompose, generating greenhouse gases (e.g., Semiletov et al., 1996a,b; Anderson et al., 2009; Shakhova et al., 2015), or be destined for burial in inland and coastal sediments. These sedimentary archives serve as long- and short-term reservoirs that attenuate greenhouse gas emissions from thawing permafrost (Vonk and Gustafsson, 2013; Semiletov et al., 2011).

The release of OM from thawing permafrost into aquatic sediments varies over time and space. A recent study showed that at the end of the last glacial, the surface active layer of terrestrial permafrost released about 4.5 Tg organic carbon (OC) per year from just the Lena watershed onto the nearby shelf, whereas current annual OC release is estimated to be only about a tenth of this (Tesi et al., 2016). In addition to active layer material, OM from deeper and older permafrost sources can also thaw and be released into the environment (Shakhova et al., 2007, 2014). This process currently dominates the delivery of terrestrial material onto the East Siberian Arctic shelf (Vonk et al., 2012; Semiletov et al., 1999) and is expected to increase due to accelerating coastal erosion rates (Günther et al., 2013).

Different permafrost OC stocks exhibit variable vulnerabilities to thaw remobilization (Schuur et al., 2015). In addition to a subsea permafrost OC stock, soils and sediments of the terrestrial northern permafrost zone store about 1300±200 Pg OC, with separate upscaling approaches applied for soil stocks (0-3m depth), deltaic sediments (full depth) and Yedoma sediments (full depth) (Hugelius et al., 2014). Yedoma sediments, a.k.a. Ice Complex Deposits (ICD) are polygenetic, ice-rich Pleistocene-aged deposits that are present in the unglaciated parts of Siberia and Alaska (Schirrmeister et al., 2011). These deposits contain roughly a quarter of the OC stored in permafrost terrain, but estimates vary from ca. 200-400 Pg C (Strauss et al., 2013; Schuur et al., 2015). The presence of massive ice wedges in ICD causes landscapes to collapse upon thaw, exposing deeper stocks of OC. This type of relatively abrupt thaw is increasing in many parts of the arctic landscape (Schuur et al., 2015). At the same time, deepening of the active layer causes gradual thaw that occurs across entire landscapes (Shiklomanov et al., 2013).

With a tool to detect and monitor different types of permafrost OM in coastal environments, one could assess (historical and spatial) variability in permafrost source input, degradation and thaw, as well as the relative degradation of different permafrost types. For example, the relative release of OC from ICD versus topsoil permafrost has earlier been distinguished and quantified through the use of dual-carbon isotopes ($\delta^{13}C$ and $\Delta^{14}C$) on bulk OC in the shelf environment of the Laptev and East Siberian Sea. It was shown that topsoil permafrost OC dominates in suspended particulate matter (Karlsson et al., 2011; 2016; Vonk et al., 2012) and ICD

permafrost OC dominates in the surface sediments (Vonk et al., 2012; Semiletov et al., 2011; 2012). Vonk et al. (2014) further showed that topsoil OC is actively degraded during horizontal transport whereas ICD permafrost OC rapidly settles. Winterfeld et al. (2015) showed, using dual-carbon isotopes on riverine material, that suspended particulate OC in the Lena Delta mostly consists of Holocene material instead of material from ICD permafrost.

This $\delta^{13}C$-$\Delta^{14}C$ dual-carbon isotope approach carries the strong advantage that it operates on the bulk OC level, thereby circumventing the "molecular-bulk upscaling challenge". This challenge relates to issues associated with upscaling from the molecular isotope level to the bulk level. These issues relate to the relative concentration (*n*-alkanes and *n*-alkanoic acids represent only a fraction of the total OC) but also to processes such as selective degradation, differences in physical association, or dispersion differences. However, the $\delta^{13}C$-$\Delta^{14}C$ approach also has drawbacks, such as a weak distinction between the $\delta^{13}C$ end-member values of Topsoil-PF versus ICD-PF. Also, the marine $\delta^{13}C$ end member values in coastal Arctic shelf waters are uncertain and may be more depleted than at mid-latitudes due to uptake of relatively depleted dissolved CO_2 values caused by cold polar water (Meyers, 1997; Tesi et al. *this special issue*) or degradation of terrestrial matter (Anderson et al., 2009; 2011; Semiletov et al., 2013; 2016), generating a potential overlap between marine and topsoil $\delta^{13}C$ end-members.

Here we propose a complementary tool to trace permafrost OC release into the coastal environment based on molecular $\delta^{2}H$ analysis on leaf waxes. We will evaluate the performance of this tool using additional geochemical data as well as the bulk $\delta^{13}C$-$\Delta^{14}C$ mixing approach. Isotopes in water molecules ($\delta^{2}H$ or $\delta^{18}O$) in glacial ice cores as well as in massive ground ice in the northern hemisphere have been used for reconstructing palaeotemperatures (e.g., Kotler and Burn, 2000; Johnson et al., 2001; Opel et al., 2011; Meyer et al., 2015; Wetterich et al., 2016) as the isotopic value of local precipitation is a function of local climate (Craig, 1961; Sachse et al., 2004; Smith and Freeman, 2006). Higher plants use water as their primary source of hydrogen during photosynthesis (Sternberg, 1988). The $\delta^{2}H$ isotope values of leaf wax *n*-alkanoic acids or *n*-alkanes are therefore reflecting the $\delta^{2}H$ isotopic value of local precipitation (e.g., Sachse et al., 2004; Sessions et al., 1999), after correction for the net fractionation during biosynthesis, and evapotranspiration (Leaney et al., 1985). Global precipitation values can vary immensely (Dansgaard, 1964) with values up to +50‰ in Eastern Africa but approaching -200‰ near the North Pole (www.iaea.org) or even below -400‰ in Antarctica (i.e. SLAP2 standard, Standard Light Antarctic Precipitation, is -427.5‰). Additionally, the fractionation between source water and plant wax molecules varies both in time and space, and can be up to -170‰ (Smith and Freeman, 2006; Sachse et al., 2004; Polissar and Freeman, 2010) but appears relatively small at higher latitudes (between -59 and -96‰; Shanahan et al., 2013; Wilkie et al., 2013; Porter et al., 2016). Differences in $\delta^{2}H$ signatures of leaf wax molecules from terrestrial regions with different (past) climates could therefore potentially be applied to derive the relative proportion of different types of thawing

permafrost in nearby coastal settings. Despite the plant fractionation associated with kinetics and plant physiology (Sachse et al., 2012), we hypothesize that δ^2H signatures of leaf wax *n*-alkanoic acids and *n*-alkanes are more depleted in OC from permafrost deposits formed during the colder Pleistocene (generally correlating with ^2H-depleted precipitation), compared to more enriched values in OC from active layer or surface permafrost formed during the warmer Holocene.

This study investigates a source-specific δ^2H signature for both ICD permafrost and recent, surface soil permafrost in Northeast Siberia. Furthermore, we explore the possibilities of using these isotopic end-member values in regional source-apportionment calculations that aim to quantify the relative contribution of different sources of permafrost OC. As permafrost thaw progresses, particularly in ice-rich permafrost such as ICD, it is increasingly important to trace the fate of remobilized and decomposing OC in the Arctic environment. Our proposed tool may be used to trace these temporal and spatial differences in OC release from permafrost thaw, as well as the extent of burial of OC in sedimentary reservoirs.

2 Methods

2.1 Sampling

A total of 18 samples were collected throughout the Siberian Arctic. Recent surface soils (n=7) and vegetation (n=2) samples were analyzed and (from here on) referred to as the "topsoil" permafrost (Topsoil-PF) sample set, whereas ICD-PF samples were obtained from ICD soil profiles (n=7) and suspended particulates from ICD formations (n=2) (Fig. 1 and Table 1). Eight offshore sediments along a shelf-slope-continental rise transect in the Laptev Sea were collected in 2014, further marine sampling details can be found in Bröder et al. (2016b).

The Topsoil-PF samples represent O and A soil genetic horizons in sites with active soil formation. The sites where chosen to represent typical soil and vegetation types in the investigated permafrost landscapes, including both taiga and tundra sites. Samples were collected by depth or soil horizon increments from open soil pits using fixed volume sampling procedures.

The ICD-PF samples were collected from vertical exposures that were excavated to expose intact permafrost. Fixed-volume samples were collected by coring horizontally into the frozen sediments to extract ICD-PF samples from consecutive depths.

For more details about sampling sites, including location, vegetation and soil types see table 1 (terminology following the U.S.D.A. Soil Taxonomy; Soil Survey Staff, 2014). Sampling was done in late summer near the time of maximum annual active layer depth, in July 2010 (ICD-8 and ICD-9; Vonk et al. (2013)) and August 2011 (Palmtag et al., 2015) for the Kolyma River region, in August 2012 for the lower Lena River and Indigirka River (Siewert et al., 2015; Weiss et al., 2015) and in August 2013

for the upper Lena River (Siewert et al., 2016). For more detailed descriptions of sample collection we refer to these references. The vegetation samples TS-8G (grass) and TS-9G (grass) were obtained from the tundra near Medvezhka River and a birch forest near Y4 stream, respectively, in July 2012.

Samples ICD-8 and ICD-9 were obtained in July 2010 at the Duvannyi Yar ICD exposure along the Kolyma River (Vonk et al., 2013). The particulate sediment samples were taken from thaw streams that were freshly formed from thawing ICD (transport time from thaw to sampling estimated to be less than 1h).

2.2 Analytical methods

Freeze-dried samples were extracted using an ASE 200 accelerated solvent extractor (Dionex Corporation, USA) using DCM/MeOH (9:1 v/v) at 80°C ($5x10^6$ Pa) (Wiesenberg et al., 2004). After the extraction, solvent-rinsed activated copper and anhydrous sodium sulfate were added to the extracts to remove sulfur and excess water, respectively. After 24 h, extracts were filtered on pre-combusted glass wool and concentrated with the rotary evaporator. Extracts were transferred into glass tubes, evaporated to complete dryness and re-dissolved in 500 µl of DCM. Lipid fractionation was performed via column chromatography using amino-propyl Bond Elut (500 mg/3 ml) to retain the acid fraction and Al_2O_3 to separate the hydrocarbon and polar fractions (Vonk et al., 2010).

Prior to the analyses, saturated *n*-alkanes (hydrocarbon fraction) were further purified using 10% $AgNO_3$ coated silica gel to retain the unsaturated fraction. The acid fraction was methylated using a mixture of HCl, MilliQ water and methanol at 80°C overnight to obtain the fatty acid methyl ester (FAME) fraction. Methylated acids were extracted with hexane and further purified using 10% $AgNO_3$ coated silica gel. The hydrocarbon and FAME fractions were quantified via gas chromatography mass spectrometry (GC–MS) in full scan mode (50-650 m/z) using the response factors of commercially available standards (Sigma-Aldrich). The GC was equipped with a 30 m×250 µm DB5-ms (0.25 µm thick film) capillary GC column. Initial GC oven temperature was set at 60°C followed by a 10°C min^{-1} ramp until a final temperature of 310°C (hold time 10 min).

The hydrogen-isotopic composition of hydrocarbon and FAME fractions was measured with continuous-flow GC - isotope ratio - MS. Purified extracts were concentrated and injected (1-2 µl) into a Thermo Trace Ultra GC equipped with a 30m×250 µm HP5 (0.25 µm thick film) capillary GC column. Oven conditions were similar to the setting used for the quantification. The conversion of organic biomarkers to elemental hydrogen was accomplished by high-temperature conversion (HTC) at 1420°C (Thermo GC Isolink). After the HTC, H_2 was introduced into the isotope ratio MS (Thermo Scientific™ Delta V™IRMS) for compound-specific determination of δ^2H values via a Thermo Conflo IV. Following a linearity test, we only used peaks with amplitude (mass 2) between 1500 and 8000 mV for the evaluation. The δ^2H values were calibrated against saturated HMW *n*-alkanes using the reference

substance mix A4 (Biogeochemical Laboratories, Indiana University). The H_3^+ factor (Sessions et al., 2001) was determined every day and stayed constant (<3 ‰/V) throughout our analyses period. Each purified extract was injected three times. FAMEs were further corrected to account for the methylation agent by comparing the hydrogen abundance of lauric acid (C_{12}-FA; i.e. 12 carbon atoms) as acid and corresponding methyl ester. The average methylation correction for lauric acid was 23.97±3.9‰ (n=4). This correction was, normalized to chain length (i.e. increasing chain lengths result in lower corrections), applied to all the FAMEs. δ^2H values of *n*-alkanes and FAMEs are reported as mean, standard deviation and weighted average.

Details of the analytical methods for extraction, work-up, and purification of the eight offshore sediment samples for biomarker analysis that are included in our source-apportionment comparison (section 4.3) can be found in Bröder et al. (2016b). The δ^2H analysis on the shelf sediments was performed in parallel with the ICD-PF and Topsoil-PF samples, according to the method described above.

2.3 Source apportionment

The compound-specific δ^2H signatures in this study were used to differentiate between the two major sources (end-members), Topsoil-PF and ICD-PF, using an isotopic mass-balance model. We used a Markov chain Monte Carlo (MCMC) approach to account for the end-member variability (Andersson et al., 2015; Bosch et al., 2015). The end-members were represented by normal distributions, with mean and standard deviations obtained from our analysis (δ^2H on TS and ICD samples) and from literature ($\delta^{13}C$ and $\Delta^{14}C$ on end-members)". For each Laptev Sea station, the isotope signatures from three different terrestrial molecular markers (long-chain *n*-alkanes C_{27}, C_{29} and C_{31}) were used jointly to improve source apportionment precision. The δ^2H signatures for the two end-members were based on our Topsoil-PF and ICD-PF samples.

The compound-specific δ^2H-based source apportionment was compared to $\Delta^{14}C/\delta^{13}C$-based analysis of bulk OC using analogous MCMC techniques (e.g., Vonk et al., 2012). The $\Delta^{14}C/\delta^{13}C$-approach allows estimation of the relative contribution of a third source, marine, which does not affect the presently investigated (terrestrial) compounds. Accounting for the marine component to OC allows direct comparison of the Holocene and Pleistocene contributions. All MCMC calculations were made using Matlab scripts (ver. 2014b) using 200,000 iterations, a burn-in phase (initial search period) of 10,000 and a data thinning of 10.

The spatial extent of ICD in the Lena River Basin was calculated by overlaying the extent of the drainage basin (from WRIBASIN: Watersheds of the World published by the World Resources Institute, www.wri.org/publication/watersheds-world) with the extent of the Yedoma Region (digitized from Romanovsky, 1993) in an equal area map projection. It was assumed that 30% of the Yedoma Region consists of intact ICD (following Strauss et al., 2013).

3 Results

3.1 Bulk geochemistry

The investigated Topsoil-PF and ICD-PF samples are, on a bulk geochemical level, very different. Mean organic carbon contents (as %OC) and total nitrogen content (as %TN) are 25±12 and 1.1±0.67 for Topsoil-PF samples, and 1.6±0.31 and 0.17±0.058 for ICD-PF samples, respectively (Table 1). This gives TOC/TN ratios of 25±8.0 for Topsoil-PF samples and 10±2.6 for ICD-PF samples. Stable carbon isotopic values of Topsoil-PF and ICD-PF samples are -27.8±1.3‰ and -25.7±0.75‰, respectively (Table 1). Radiocarbon ages were unfortunately only available for a few ICD samples, and ranged between 17 and 28 ^{14}C ka (Table 1).

3.2 Molecular geochemical composition

Long-chain *n*-alkanes and *n*-alkanoic acids are abundant in epicuticular waxes and therefore indicative for a source of higher plants (Eglinton and Hamilton, 1967). Concentrations of individual long-chain *n*-alkanes in Topsoil-PF samples ranged from 1 to 340 µg/gOC (C_{21}-C_{33}; Table 2) with an average chain length of 28±1.6. The sum of high-molecular weight (HMW) *n*-alkanes (>C_{21}) for Topsoil-PF samples was 418^{612}_{280} µg/gOC (median with interquartile range) and the most abundant *n*-alkanes added up to 214^{494}_{148} µg/gOC (sum of C_{25}-C_{27}-C_{29}-C_{31}) (Table 4, Fig. 2a). For ICD-PF samples, the individual concentrations of long-chain *n*-alkanes were between 4 and 160 µg/gOC, and the average chain length 27±0.7 (Table 2). The sum of high-molecular weight *n*-alkanes, and most abundant *n*-alkanes were 698^{806}_{630} µg/gOC and 347^{405}_{323} µg/gOC, respectively (Table 4, Fig. 2a). The carbon preference index (CPI), a molecular ratio indicative for degradation status with values >5 typical for fresher terrestrial material and values approaching 1 typical for more degraded samples (Hedges and Prahl, 1993), showed values for Topsoil-PF samples of 7.3±3.6 (average±standard deviation) and ICD-PF samples of 3.6±0.8 (CPI C_{23}-C_{31}; Table 4, Fig. 2c). The $C_{25}/(C_{25}+C_{29})$ ratio, indicative for the input of peat moss (*Sphagnum sp.*) material (Vonk and Gustafsson, 2009; *Sphagnum* values 0.72, higher plants 0.07; Nott et al., 2000) was 0.33±0.22 (average±standard deviation) and 0.34±0.05 for Topsoil-PF and ICD-PF samples, respectively (Table 4). Another commonly used *Sphagnum* proxy (Bush and McInerney, 2013), $C_{23}/(C_{23}+C_{29})$, resulted in a sharper contrast between ICD-PF and Topsoil-PF samples (0.39±0.13 and 0.25±0.23, respectively; Fig. 2e and Table 4).

Long-chain *n*-alkanoic acids (C_{22} and above) were abundant in concentrations between 0.122 and 2670 µg/gOC for individual homologues in topsoils, with the sum of HMW *n*-alkanoic acids (>C_{22}) being 6397^{7454}_{3167} µg/gOC (median and IQR) and the most abundant *n*-alkanoic acids (sum of C_{22}-C_{24}-C_{26}-C_{28}) adding up to 4700^{6092}_{2670} µg/gOC (Table 3, 4 and Fig. 2b). ICD-PF samples contained individual long-chain *n*-alkanoic acids in 2.17 and 18700 µg/gOC (Table 2), a sum of HMW *n*-alkanoic acids of 8290^{11430}_{6290} µg/gOC, and the sum of most abundant, even *n*-alkanoic acids of 6630^{8790}_{5285}µg/gOC (Table 4). Topsoil-PF and ICD-PF samples had average chain lengths of 24.1±1.1 and 24.3±0.59, and CPI (C_{22}-C_{28}) values of 5.9±2.7 (average±standard

deviation) and 5.0±1.6, respectively (Table 4). Shorter-chain *n*-alkanoic acids C_{16} and C_{18} are produced in basically all types of life in soils or aquatic environments, and are not specific for higher plants. Topsoil-PF contained C_{16} and C_{18} homologues in concentrations between 220 and 4600 µg/gOC, and ICD-PF samples between 200 and 10400 µg/gOC (Table 3).

Degradation of organic matter involves the loss of functional groups, e.g. the loss of carboxylic acids (Meyers and Ishiwatari, 1993). A high ratio of HMW *n*-alkanoic acids over HMW *n*-alkanes in a sample therefore implies a relatively fresh, less degraded, status (i.e. relatively more functional groups present). For Topsoil-PF samples, the HMW *n*-alkanoic acid/HMW *n*-alkane ratio varied between 5.6 and 25 with an average value of 13±7.6, whereas ICD-PF samples varied between 7.6 and 140 with an average value of 29±43 (Table 4, Fig. 2f).

3.3 Molecular isotopic composition

We measured δ^2H values in long-chain *n*-alkanes and *n*-alkanoic acids between -119 and -313‰ (Fig. 3, Table 5). Mean values for HMW *n*-alkanes (C_{25}-C_{27}-C_{29}-C_{31}) were between -201 and -247‰ for Topsoil-PF samples and between -221 and -297‰ for ICD-PF samples, with consistently lower δ^2H for longer chain lengths. For HMW *n*-alkanoic acids (C_{22}-C_{24}-C_{26}-C_{28}) mean δ^2H values were between -203 and -236‰ for Topsoil-PF samples and between -261 and -278‰ for ICD-PF samples (Table 5). The decrease in δ^2H values with increasing chain length is less distinct for *n*-alkanoic acids but one can observe a decrease of around 25-30‰ from C_{22} to C_{26} (Fig. 3). For ICD-PF samples, the isotopic depletion for the average of the three most abundant *n*-alkanes is comparable to the average for *n*-alkanoic acids, whereas in Topsoil-PF samples, the isotopic depletion for the three most abundant *n*-alkanes is a bit larger than for *n*-alkanoic acids (Fig. 4).

4 Discussion

4.1 Using bulk geochemistry and molecular proxies

Bulk geochemical and isotopic analysis, as well as analysis of molecular proxies remained inconclusive in distinguishing between the two investigated sources in this study. Topsoil-PF samples have a higher organic content, higher TOC/TN values (representing fresh, higher plant material; Meyers, 1994) and more depleted $\delta^{13}C$ values (indicative for terrestrial C3 plants; Meyers, 1997) than ICD-PF samples, suggesting that these samples indeed trace a fresh soil and/or vegetation source (Table 1). The $\delta^{13}C$ values of a larger ICD-PF and Topsoil-PF dataset have earlier been summarized (Vonk et al., 2012 and references therein; Schirrmeister et al., 2011) giving values of -26.3±0.67‰ (n=374) and -28.2±2.0‰ (n=30), respectively. Our values (Table 1) are in a similar range. Despite the differences between these two sources in their bulk geochemistry, it is hard to use these parameters for source distinction as their variability is fairly high, and their behavior in the environment is not conservative, but e.g. affected by degradation processes. On a molecular geochemical level the two investigated sources are virtually indistinguishable as

there is a considerable variation in molecular concentrations and proxy values (Fig. 2). Only one of the tested parameters, the CPI C_{23}-C_{31} of *n*-alkanes, showed a statistically significantly different value for the two investigated sources.

4.2 Evaluation of molecular δ^2H values as a source end-member

To alleviate the difficulty to distinguish between Topsoil-PF and ICD-PF with just bulk and molecular geochemical characteristics, we explore the δ^2H values of leaf wax molecules (i.e. long chain *n*-alkanoic acids and *n*-alkanes) to differentiate between their relative source contributions. The overall mean δ^2H of the four most abundant *n*-alkanoic acids is -231±29‰ and -271±13‰ for Topsoil-PF and ICD-PF samples, respectively. These values compare well with available literature (Fig. 5). Pautler et al. (2014) measured δ^2H values on C_{29} *n*-alkanes in modern soils of the Yukon, Canada of -252±9.1‰ (n=4) and aged soil δ^2H values of -269±8.6‰ (n=13; 24-25 ^{14}C-ka ago) and -273±16.4‰ (n=9; for MIS 4, ~70 ^{14}C-ka ago). Yang et al. (2011) also reported C_{29} *n*-alkane δ^2H values for modern vegetation from Alaska and Arctic Canada with an average value of -252±43‰ (n=8). Zech et al. (2011) reported values of C_{29} *n*-alkanes collected from a permafrost exposure along the Tumara River in northeast Siberia, with an average value of -266±7.5‰ (n=23) for glacial paleosoils and -247±9.4‰ (n=17) for interglacial paleosoils. Our values for C_{29} *n*-alkanes for Topsoil-PF (-246±13‰; n=9) and ICD-PF (-280±12‰; n=9) are in a similar range (Fig. 5). For C_{28} *n*-alkanoic acids, Wilkie et al. (2013) measured -252±8.7‰ (n=6) for modern vegetation in northeast Siberia, whereas Porter et al. (2016) measured -269±2.7‰ (n=7) for ca. 31 cal ka BP old soils in the Yukon. Compared to these studies, our values for C_{28} *n*-alkanoic acids are somewhat more enriched for Topsoil-PF with -220±15‰ (n=7) but roughly in the same range for ICD-PF with -267±16‰ (n=9).

The mean isotopic difference between the most abundant *n*-alkanoic acids of the two investigated sources is around 40‰ (δ^2H values of -231±29‰ and -271±13‰ for Topsoil-PF and ICD-PF samples, respectively). Despite the relatively large standard deviations, the isotopic differences are statistically significant for each of the *n*-alkanoic acids individually (C_{22}, C_{24}, C_{26}, C_{28}; Fig. 3). The isotopic differences between the two sources for the mean value of the four most abundant *n*-alkanes is 35‰, with a mean value of -229±33‰ and -264±34‰ for Topsoil-PF and ICD-PF samples, respectively. Here, the individual *n*-alkane isotopic signatures are statistically significantly different for C_{27}, C_{29}, C_{31} (Fig. 3) in Topsoil-PF and ICD-PF samples. The selection and application of individual chain length δ^2H values as end-members, in contrast to mean chain length values, might be more appropriate for several reasons; (i) to reduce variability (δ^2H ranges for C_{29} and C_{31} *n*-alkanes and C_{22} and C_{24} *n*-alkanoic acids are relatively low; Fig. 3), (ii) to target the most abundant species (C_{29} and C_{31} *n*-alkanes are generally more abundant in soils and ICD-PF compared to shorter chain lengths; Table 2), and (iii) to make use of the largest dynamic range between source end-member values (C_{31} *n*-alkane δ^2H values of Topsoil-PF and ICD-PF differ by 50‰). Based on these arguments, the C_{28} *n*-alkanoic acid and the C_{29} or C_{31} *n*-alkanes are most appropriate to use for source-apportionment. The available

previous studies (Fig. 5) have also selected these chain lengths (C_{28} *n*-alkanoic acid and C_{29} *n*-alkanes) for proxy development.

The use of molecular δ^2H values as tracers of terrestrial material in a marine or coastal setting has the advantage that it avoids uncertainty issues related to definition of the marine end-member. On the other hand, the inherent bulk-upscaling challenge of any molecular proxy, is a disadvantage of the δ^2H approach as it introduces unknowns related to the molecular-bulk upscaling effort (e.g. taking into account sorting and recalcitrance; discussed in depth in 4.3). We also want to emphasize that δ^2H leaf wax values in the two studied end-member sets (Topsoil-PF vs. ICD-PF) largely depend on the climate (warm vs. cold) and continentality (near the coast vs. further inland) during plant formation, and associated differences in fractionation mechanisms. Consequently, when δ^2H values in samples are used for source-apportionment, this may represent the fraction leaf wax produced in cold vs. warm conditions (as well as degree of continentality), and not necessarily the fraction Topsoil-PF vs. ICD-PF.

Finally, we realize that the amount of soil and ICD samples analyzed in this study is limited, and want to point out that the results may change when more data are analyzed in the near future. Additionally, studies have shown that the δ^2H signature of ice within ICD permafrost deposits can range from roughly -150‰ to -260‰ depending on the type of ice (wedge ice vs. pore or texture ice) as well as the period of formation (different Pleistocene cold stages) (Opel et al., 2017 and references therein). The source of water (i.e. type of ice) and age of the deposit will therefore influence the *n*-alkane or *n*-alkanoic acid δ^2H signal. However, regardless of the natural variability associated with the processes mentioned above, both ICD and texture-ice isotopic compositions appear to reflect long-term climate changes (Opel et al., 2017; Schwamborn et al., 2006; Dereviagin et al., 2013; Porter et al., 2016) which, likely, were also captured in the *n*-alkane or *n*-alkanoic acid δ^2H signal. Unfortunately, we do not have ^{14}C-ages available for all ICD samples, so cross-referencing to published stratigraphies in the region is not possible. Coastal sediments, however, will represent a mixture of material released from different depths, outcrops, and stratigraphies within the catchment or coast. For source-apportionment applications, we reason that a growing body of leaf wax δ^2H end-member data from the ICD region can overcome the variability issues highlighted above.

4.3 Comparison with ^{13}C-^{14}C source-apportionment: a case-study

Bulk OC dual-carbon isotope data provide a quantitative apportionment tool to assess the relative contributions of Topsoil-PF vs. ICD-PF. Here, we present a case-study of a shelf-slope transect in the Laptev Sea (Fig. 1) where both these source-apportionment tools for the first time can be applied, compared and evaluated. The shelf-slope transect of eight surface sediment samples stretches over 600 km from the nearshore zone (72.7°N, <10m water depth) to the continental rise (78.9°N,

>3000m depth) (Table 6). More molecular and bulk geochemical characteristics of these samples can be found in Bröder et al. (2016b).

The $\delta^{13}C$-$\Delta^{14}C$ source-apportionment uses three end-members (marine, Topsoil-PF, and ICD-PF). End-member values are based on previously published values (Tesi et al., 2016); with a $\delta^{13}C$ value of -27.0±1.2‰ (n=38; Rodionow et al., 2006; Tesi et al., 2014; Gundelwein et al., 2007; Bird et al., 2002) for Topsoil-PF, and -26.3±0.67‰ (n=374; Vonk et al., 2012; Schirrmeister et al., 2011) for ICD-PF. The Topsoil-PF $\Delta^{14}C$ endmember was defined as -232±147‰ (n=29; Winterfeld et al., 2015; Jasinski et al., 1998; Kaiser et al., 2007; Höfle et al., 2013; Palmtag et al., 2015). For ICD-PF we used a $\Delta^{14}C$ value of -940±84‰ (n=300; Vonk et al., 2012 and references therein). The marine end-member value was -21.0±2.6‰ (n=10; Panova et al., 2015) and -50.4±12‰ (n=10; Panova et al., 2015) for $\delta^{13}C$ and $\Delta^{14}C$, respectively. Calculations were made using a Markov chain Monte Carlo approach (see 2.3).

For $\delta^{2}H$ source-apportionment there is no need to include a marine end-member as marine organisms do not produce long-chain *n*-alkanes or *n*-alkanoic acids. We were unfortunately only able to analyze *n*-alkanes in the shelf-slope transect samples, and no *n*-alkanoic acids, due to limitations in sample volume. We used the $\delta^{2}H$ values of the C_{27}, C_{29} and C_{31} *n*-alkanes, individually. In other words, these three chain lengths are taken as independent markers, providing an overdetermined system (i.e. two sources defined with three different markers). This is more representative than using the average (concentration-weighted) $\delta^{2}H$ value for these *n*-alkanes as the end-member values for each chain length are different. For Topsoil-PF we used -215±39‰, -246±13‰, and -247±23‰ for C_{27}, C_{29} and C_{31} *n*-alkanes, and for ICD-PF we applied -259±18‰, -297±15‰, and -282±13‰ for C_{27}, C_{29} and C_{31} *n*-alkanes, respectively (see also Table 5). Afterwards, we averaged the three end-member contributions derived from the three calculations for each station, thereby taking the variability introduced by the end-members into account.

The source apportionment of OC from Topsoil-PF and ICD-PF to surface sediments along the Laptev Sea transect differ between the bulk $\delta^{13}C$-$\Delta^{14}C$ and leaf wax $\delta^{2}H$ approaches (Table 6). The former approach suggests Topsoil-PF contributions between 21-70%, generally decreasing offshore, and, consequently, ICD-PF contributions of 30-79%, generally increasing offshore. The latter (leaf wax $\delta^{2}H$) approach results in a more extreme division of sources with Topsoil-PF contributions of 83-91% and ICD-PF contributions of 9-17%, with similar patterns nearshore and offshore (Table 6). A contribution of 9-17% may seem more in line with the estimated extent of ICD in the Lena River basin: 12% of the basin falls within the Yedoma Region (as defined by Romanovsky, 1993) and about 3% consists of intact ICD (see section 2.3). However, the cross-shelf sites are also strongly influenced by coastal and/or subsea erosion (Karlsson et al. 2011; Vonk et al., 2012; Semiletov et al., 2012; 2016) so the catchment characteristics are only one part of the story. It is challenging to interpret the differences between the two proxies but we elaborate below on potential reasons.

Assumptions in the bulk $\delta^{13}C$-$\Delta^{14}C$ approach may affect these results. First, the outcome of the bulk $\delta^{13}C$-$\Delta^{14}C$ approach is sensitive to the definition of the marine end-member. Changes in the currently used $\delta^{13}C$ and $\Delta^{14}C$ value of the marine end-member of the East Siberian Arctic Shelf (n=10; Panova et al., 2015) would likely alter the relative Topsoil-PF and ICD-PF contributions. The currently used standard deviation for the $\delta^{13}C$ marine end-member is 2.6‰, which is much higher than the values for the terrestrial end-members. Second, lateral transport time enroute the shelf-slope transect (>600 kilometers) causing potentially significant aging of sediments and its organic carbon is not accounted for in the source-apportionment. Lateral transport time results in older surface OC ages on the shelf, compared to those at the initial coastal deposition. Without correcting for this factor, the source-apportionment will generate lower contributions of the (younger) Topsoil-PF component. In an attempt to estimate this effect, we recalculated (similar to Bröder et al. 2016a) the relative source contributions of Topsoil-PF, ICD-PF (and marine) with the bulk $\delta^{13}C$-$\Delta^{14}C$ approach with the assumption that the Topsoil-PF ^{14}C age would be subject to a cross-shelf lateral transport time of 5000 yrs. We assumed a linear aging along the transect based on distance from the coast, with a maximum value of 5000 yrs aging at station SW-01. This resulted in Topsoil-PF contributions that were up to 20% higher (for the deepest stations) compared to the source-apportionment where lateral transport time was unaccounted for (Table 6; Fig. 6).

Assumptions in the leaf wax $\delta^{2}H$ source-apportionment approach could potentially also impact the outcomes, and hence differences with the bulk $\delta^{13}C$-$\Delta^{14}C$ results. First, there is an inherent assumption related to the molecular to bulk level upscaling challenge. We assume that the physical association of *n*-alkanes in different source end-members (Topsoil-PF vs. ICD-PF) as well as their fractionation in the coastal system is similar. However, previous research has shown that *n*-alkanes behave rather differently upon their release into coastal waters; *n*-alkanes originating from surface soil or vegetation debris are not bound to minerals and remain in suspension during transport while being actively degraded, whereas *n*-alkanes originating in deeper mineral soils settle quickly and are protected from extensive degradation (Vonk et al., 2010). It is possible that most of the *n*-alkanes in the Laptev Sea sediment transect originate in (deeper) mineral soils. An effect of physical association, as well as the potential effect of hydrodynamic sorting patterns (Tesi et al., 2016) on the leaf wax $\delta^{2}H$ values of both sources could impact the source-apportionment. Another factor that can introduce a bias in our leaf wax $\delta^{2}H$ approach is a proton exchange of the C-bound H-atoms in *n*-alkanes with environmental water, either from in situ sources (soil water) or during transport (river or ocean water, or sediment pore water). As there is no evidence for such exchange in young (<1 million years), cold sediments (Sessions et al., 2004) we suspect this process may be minimal in our samples (and end-members).

When accounting for an estimated lateral transport time, the difference in estimates of source contribution by the two different approaches (bulk $\delta^{13}C$-$\Delta^{14}C$ and leaf wax

δ^2H) increases offshore, from about a 25% difference near the coast to a 40% difference at stations SW-01 and SW-03. This increasing offset between the results of the two end-member mixing methods may be caused by several factors such as variability in the marine end-member (e.g. due to changes in seasonal ice cover), a selective degradation (of the topsoil OC) enroute that introduces a source bias or isotopic fractionation, or remaining factors related to the lateral transport time (incorrect assumption of 5000 years, non-linear aging along transect). These differences highlight that both source-apportionment tools still could be fine-tuned further by (i) increasing the sample size of sources to reduce end-member uncertainties, (ii) continuous adjustments in end-member values and Markov chain Monte Carlo calculations based on latest knowledge, and (iii) assuring regional testing and verification of the method when applied to new environments.

5 Conclusions

Leaf wax δ^2H values in samples from aquatic recipient environments can be used to source-apportion the incoming terrestrial OC into two end-members; a Pleistocene ICD permafrost source and a younger, Holocene, topsoil source. Mean isotopic values of the C_{29} *n*-alkane, C_{31} *n*-alkane, and C_{28} *n*-alkanoic acid showed a dynamic, statistically significant range of 34, 50 and 46‰ between Topsoil-PF and ICD-PF samples, respectively, with ICD-PF samples being consistently more depleted indicative of formation during the colder and drier Pleistocene.

A case-study where we tested two isotopic proxies (leaf wax δ^2H and bulk $\delta^{13}C$-$\Delta^{14}C$) to calculate the relative terrestrial source contribution of Topsoil-PF and ICD-PF along a Laptev Sea surface sediment transect, showed that the two proxies yield variable results but overall generate similar trends offshore. We reason that variability is caused by factors such as lateral transport time, remaining uncertainties in end-member definition, or environmental factors such as physical association.

Both methods (leaf wax δ^2H and bulk $\delta^{13}C$-$\Delta^{14}C$) bring along their inherent disadvantages and advantages. The molecular approach has the distinct advantage that it circumvents the uncertainties that are associated with marine end-member definition in the case of bulk OC mixing model analysis. However, application of molecular δ^2H in source-apportionment studies brings along challenges related to the molecular-bulk upscaling step. Bulk $\delta^{13}C$-$\Delta^{14}C$ source-apportionment, on the other hand, has the advantage to operate on a bulk and perhaps more representative level, but is hampered by remaining uncertainties associated with the marine end-member.

This study shows that δ^2H of leaf wax molecules has the potential to be used in quantitative source-apportionment studies of thawing permafrost in coastal or marine settings. It can serve as an alternative or complementary approach to the commonly applied bulk $\delta^{13}C$-$\Delta^{14}C$ method. We recommend continuing data collection and optimization of end-member definition and calibration. Refining the molecular δ^2H proxy presented here will be beneficial in pinpointing the location and extent of OC release from thawing permafrost in the coastal or fluvial environment. With

enhanced Arctic warming and associated intensification of permafrost thaw, constraining the amount and fate of permafrost OC release will help to assess the magnitude of the permafrost carbon feedback to climate warming.

Data availability

All data are available in Tables 1 through 6, as well as Supplementary Table S1.

Acknowledgements

We would like to acknowledge Robert Spencer, Sergey Davydov, Anya Davydova, Ekatarina Bulygina, Peter Kuhry, Matthias Siewert, Juri Palmtag, Niels Weiss, Martin Kruså, Volker Brüchert, Pete Hill, Vladimir Mordukhovich, Alexander Charkin, Deniz Kosmach, Per Andersson, and sampling crew and personnel of IB Oden and RV Yakob Smirnitskyi for help with sample collection in the field. Financial support has been provided by the Dutch NWO (Veni #863.12.004), US-NSF (Polaris Project #1044610), the Bolin Centre for Climate Research, the Knut and Alice Wallenberg Foundation (SWERUS-C3 Program; KAW #2011.0027), the Swedish Research Council (VR #621-2004-4039 and 621-2007-4631), the Russian Science Foundation (#15-17-20032 to O. D.), the Nordic Council of Ministers Cryosphere-Climate-Carbon Initiative (project Defrost, #23001), the European Research Council (ERCAdG project CC-TOP #695331 to Ö.G.). This study was supported by the Delta Facility of the Faculty of Science, Stockholm University. GH would like to acknowledge funding from ESF-CryoCarb and EU FP7-PAGE21 projects for topsoil and ICD sample collection. The ISMAR publication ID is #1931.

Author contributions

Land-based samples were collected by GH and JEV, ship-based samples were collected by IS, OD, ÖG, TT, LB, and JEV. Laboratory analysis was performed by LB, TT, and HH. Markov chain Monte Carlo simulations were run by AA. The manuscript was written by JEV with input of all co-authors.

References

Anderson, L. G., Jutterström, S., Hjalmarsson, S., Wåhlström, I., and Semiletov, I.P.: Out-gassing of CO_2 from Siberian Shelf seas by terrestrial organic matter decomposition, Geophys. Res. Lett. 36, L20601, doi:10.1029/2009GL040046, 2009.

Anderson, L.G., Björk, G., Jutterström, S., Pipko, I., Shakhova, N. Semiletov, I. and Wåhlström, I.: East Siberian Sea, an Arctic region of very high biogeochemical activity, Biogeosciences, 8, 1745-1754, doi:10.5194/bg-8-1745-2011, 2011.

Andersson, E., Deng, J., Du, K., Zheng, M., Yan, C., Sköld, M., and Gustafsson, Ö.: Regionally-varying combustion sources of the January 2013 severe haze events over Eastern China, Environ. Sci. Technol. 49(4), 2038-2043, doi: 10.1021/es503855e, 2015.

Bird, M. I., Santruckova, H., Arneth, A., Grigoriev, S., Gleixner, G., Kalaschnikov, Y. N., Lloyd, J., and Schulze, E.-D.: Soil carbon inventories and carbon-13 on a latitude transect in Siberia, Tellus, 54B, 631-641, 2002.

Bröder, L., Tesi, T., Salvado, J.A., Semiletov, I.P., Dudarev, O.V., and Gustafsson, Ö.: Fate of terrigenous organic matter across the Laptev Sea from the mouth of the Lena River to the deep sea of the Arctic interior, Biogeosciences 13, 5003, 5019., doi:10.5194/bg-13-5003-2016, 2016b.

Bröder, L., Tesi, T., Andersson, A., Eglinton, T.I., Semiletov, I.P., Dudarev, O.V., Roos, P., and Gustafsson, Ö.: Historical records of organic matter supply and degradation status in the East Siberian Sea, Org. Geochem. 91, 16-30, doi:10.1016/j.orggeochem.2015.10.008, 2016a.

Bosch, C., Andersson, A., Kruså, M., Bandh, C., Hovorkova, I., Klanova, J., Knowles, T. D. J., Pancost, R. D., Evershed, R. P., and Gustafsson, Ö.: Source apportionment of polycyclic aromatic hydrocarbons in central European soils with compound-specific triple isotopes ($\delta^{13}C$, $\Delta^{14}C$, and $\delta^{2}H$), Environ. Sci. Technol. 49(13), 7657-7665, doi:10.1021/acs.est.5b01190, 2015.

Bush, R.T., and McInerney, F..A.: Leaf wax n-alkane distributions in and across modern plants: Implications for paleoecology and chemotaxonomy, Geochim. Cosmochim. Ac. 117, 161-179, 2013.

Craig, H.: Isotopic variations in meteoric waters, Science 133: 1702–1703, 1961.

Dansgaard, W.: Stable isotopes in precipitation, Tellus, 16, 436– 438, 1964.

Eglinton, G., and Hamilton, R.J.: Leaf epicuticular waxes, Science 156, 1322-1335, 1967.

Gundelwein, A., Mueller-Lupp, T., Sommerkorn, M., Haupt, E. T. K., Pfeiffer, E. M., and Wiechmann, H.: Carbon in tundra soils in the Lake Labaz region of arctic Siberia, Eur. J. Soil Sci., 58, 1164-1174, 2007.

Günther, F., Overduin, P.P., Sandakov, A.V., Grosse, G., and Grigoriev, M.N.: Short- and long-term thermo-erosion of ice-rich permafrost coasts in the Laptev Sea region, Biogeosciences, 10, 4297-4318, doi:10.5194/bg-10-4297-2013, 2013.

Hedges, J.I., and Prahl, F.G.: Early diagenesis: consequences for applications of molecular biomarkers, in *Organic Geochemistry: principles and applications.* Engel, M.H., and Macko, S.A. (ed.). Plenum Press, New York. pp 237-253, 1993.

Höfle, S., Rethemeyer, J., Mueller, C. W., and John, C.: Organic matter composition and stabilization in a polygonal tundra soil of the Lena Delta, Biogeosciences, 10, 3145-3158, doi:10.5194/bg-10-3145-2013, 2013

Hugelius, G. Strauss, J., Zubrzycki, S., Harden, J. W., Schuur, E. A. G., Ping, C.-L., Schirrmeister, L., Grosse, G., Michaelson, G. J., Koven, C. D., O'Donnell, J. A., Elberling, B., Mishra, U., Camill, P., Yu, Z., Palmtag, J., and Kuhry, P.: Estimated stocks of circumpolar permafrost carbon with quantified uncertainty ranges and identified data gaps, Biogeosciences 11, 6573-6593, doi:10.5194/bg-11-6573-2014, 2014.

Jasinski, J. P. P., Warner, B. G., Andreev, A. A., Aravena, R., Gilbert, S. E., Zeeb, B. A., Smol, J. P., and Velichko, A. A.: Holocene environmental history of a peatland in the Lena River valley, Siberia, Can. J. Earth Sci., 35, 637-648, 1998.

Johnsen, S. J., Dahl-Jensen, D., Gundestrup, N., Steffensen, J. P., Clausen, H. B., Miller, H.: Oxygen isotope and palaeotemperature records from six Greenland ice-core stations: Camp Century, Dye-3, GRIP, GISP2, Renland and NorthGRIP, J. Quat. Sci. 16, 299-307, doi:10.1002/jqs.622, 2001.

Kaiser, C., Meyer, H., Biasi, C., Rusalimova, O., Barsukov, P., and Richter, A.: Conservation of soil organic matter through cryoturbation in arctic soils in

691 Siberia, J. Geophys. Res.-Biogeosciences, 112, G2, doi:10.1029/2006JG000258,
692 2007.
693 Karlsson, E. S., Charkin, A., Dudarev, O., Semiletov, I., Vonk, J. E., Sanchez-Garcia, L.,
694 Andersson, A., and Gustafsson, O.: Carbon isotopes and lipid biomarker
695 investigation of sources, transport and degradation of terrestrial organic matter
696 in the Buor-Khaya Bay, SE Laptev Sea, Biogeosciences 8, 1865-1879,
697 doi:10.5194/bg-8-1865-2011, 2011.
698 Karlsson, E. S., Gelting, J., Tesi, T., van Dongen, B., Andersson, A., Semiletov, I.,
699 Charkin, Al., Dudarev, O., and Gustafsson, Ö.: Different sources and degradation
700 state of dissolved, particulate, and sedimentary organic matter along the Eurasian
701 Arctic coastal margin, Global Biogeochem. Cycles, 30, 898-919,
702 doi:10.1002/2015GB005307, 2016.
703 Kotler, E., and Burn, C. R.: Cryostratigraphy of the Klondike "muck" deposits,
704 westcentral Yukon Territory, Can. J. Earth Sci. 37, 849-861, doi:10.1139/e00-013,
705 2000.
706 Leaney, F. W., Osmond, C. B., Allison, G. B., and Ziegler, H.: Hydrogen-isotope
707 composition of leaf water in C-3 and C-4 plants - its relationship to the hydrogen
708 isotope composition of dry-matter, Planta 164 (2), 215-220, 1985.
709 Meyer, H., Opel, T., Laepple, T., Dereviagin, A.Y., Hoffmann, K., and Werner, M.: Long-
710 term winter warming trend in the Siberian Arctic during the mid- to late
711 Holocene, Nat. Geosci. 8, 122-125, doi:10.1038/ngeo2349, 2015.
712 Meyers P. A., Ishiwateri R.: Lacustrine organic geochemistry – an overview of
713 indicators of organic matter sources and diagenesis in lake sediments, Org.
714 Geochem. 20, 867-900, doi:10.1016/0146-6380(93)90100-P, 1993.
715 Meyers, P. A.: Preservation of elemental and isotopic source identification of
716 sedimentary organic matter, Chem. Geol. 114, 289-302, doi:10.1016/0009-
717 2541(94)90059-0, 1994.
718 Meyers, P. A.: Organic geochemical proxies of paleoceanographic, paleolimnologic
719 and paleoclimatic processes, Org. Geochem. 27, 213-250, doi:10.1016/S0146-
720 6380(97)00049-1, 1997.
721 Nott, C. J., Xie, S., Avsejs, L. A., Maddy, D., Chambers, F. M., Evershed, R. P.: *n*-Alkane
722 distributions in ombotrophic mires as indicators of vegetation change related to
723 climatic variation, Org. Geochem. 31, 231-235, doi:10.1016/S0146-
724 6380(99)00153-9, 2000.
725 Opel, T., Dereviagin, A. Y., Meyer, H., Schirrmeister, L., and Wetterich, S.:
726 Palaeoclimatic information from stable water isotopes of Holocene ice wedges on
727 the Dmitrii Laptev Strait, Northeast Siberia, Russia, Permafrost Periglacial
728 Process., 22, 84-100, 10.1002/ppp.667, 2011.
729 Opel, T., Wetterich, S., Meyer, H., Dereviagin, A.Y., Fuchs, M.C., and Schirrmeister, L.:
730 Ground-ice stable isotopes and cryostratigraphy reflect late Quaternary
731 palaeoclimate in the Northeast Siberian Arctic (Oyogos Yar coast, Dmitry Laptev
732 Strait), Clim. Past Discuss., doi:10.5194/cp-2017-1, 2017.
733 Palmtag J., Hugelius G., Lashchinskiy N., Tamstorf M.P., Richter A., Elberling B. and
734 Kuhry, P.: Storage, Landscape Distribution, and Burial History of Soil Organic
735 Matter in Contrasting Areas of Continuous Permafrost, Arctic, Antarctic, and Alpine
736 Research, 47(1), 71-88, doi: http://dx.doi.org/10.1657/AAAR0014-027, 2015.

737 Polissar, P. J., and Freeman, K. H.: Effects of aridity and vegetation on plant-wax dD in
738 modern lake sediments, Geochim. Cosmochim. Ac. 74, 5785-5797,
739 doi:10.1016/j.gca.2010.06.018, 2010.
740 Panova, E., Tesi, T., Pearce, C., Salvado, J. A., Karlsson, E. S., Kruså, M., Semiletov, I. P.,
741 and Ö. Gustafsson: Geochemical compositional differences of the supramicron
742 plantkon-dominated fraction in two regimes of the Marginal Ice Zone (MIZ) of the
743 outer East Siberian Arctic Shelf, AGU Fall meeting 2015 abstract, 2015.
744 Pautler, B. G., Reichart, G.-J., Sanborn, P. T., Simpson, M. J., Weijers, J. W. H.:
745 Comparison of soil derived tetraether membrane lipid distributions and plantwax
746 dD compositions for reconstruction of Canadian Arctic temperatures,
747 Palaeogeogr. Palaeoclimatol. Palaeoecol. 404, 78-88,
748 doi:10.1016/j.palaeo.2014.03.038, 2014
749 Porter, T. J., Froese, D. G., Feakins, S. J., Bindeman, I. N., Mahoney, M. E., Pautler, B. G.,
750 Reichart, G.-J., Sanborn, P. T., Simpson, M. J., and Weijers, J. W. H.: Multiple water
751 isotope proxy reconstruction of exteremely low last glacial temperatures in
752 Eastern Beringia (Western Arctic), Quat. Sci. Rev. 137, 113-125,
753 doi:10.1016/j.quascirev.2016.02.006, 2016.
754 Rodionow, A., Flessa, H., Kazansky, O., and Guggenberger, G.: Organic matter
755 composition and potential trace gas production of permafrost soils in the forest
756 tundra in northern Siberia, Geoderma, 135, 49-62, 2006.
757 Romanovsky, N. N.: Fundamentals of the cryogenesis of the lithosphere. University
758 Press, Moscow, pp. 1-336 (in Russian), 1993.
759 Sachse, D., Radke, J., and Gleixner, G.: Hydrogen isotope ratios of recent lacustrine
760 sedimentary n-alkanes record modern climate variability, Geochim. Cosmochim.
761 Ac., 68, 4877–4889, doi:10.1016/j.gca.2004.06.004, 2004.
762 Schuur, E. A. G., McGuire, A. D., Schädel, C., Grosse, G., Harden, J. W., Hayes, D. J.,
763 Hugelius, G., Koven, C. D., Kuhry, P., Lawrence, D. M., Natali, S. M., Olefeldt, D.,
764 Romanovsky, V. E., Schaefer, K., Turetsky, M. R., Treat, C. C., and Vonk, J. E.:
765 Climate change and the permafrost carbon feedback, Nature, 250, 171-178,
766 doi:10.1038/nature14338, 2015.
767 Schirrmeister, L. Kunitsky, V. V., Grosse, G., Wetterich, S., Meyer, H., Schwamborn, G.,
768 Babiy, O., Derevyagin, A., and Siegert, C.: Sedimentary characteristics and origin of
769 the Late Pleistocene Ice Complex on north-east Siberian Arctic coastal lowlands
770 and islands – A review, Quatern. Int. 241, 3-25, doi:10.1016/j.quaint.2010.04.004,
771 2011.
772 Semiletov I.P., Pipko I.I., Shakhova N.E., Dudarev O.V., Pugach S.P., Charkin A.N., McRoy
773 C.P., Kosmach D., and Gustafsson, Ö: Carbon transport by the Lena River from its
774 headwaters to the Arctic Ocean, with emphasis on fluvial input of terrestrial
775 particulate organic carbon vs. carbon transport by coastal erosion, Biogeosciences,
776 8, 2407-2426, 2011.
777 Semiletov I.P., Shakhova N. E., Sergienko V.I., Pipko I.I., and O. Dudarev: On Carbon
778 Transport and Fate in the East Siberian Arctic Land-Shelf-Atmosphere System,
779 Environment Res. Lett., 7, doi:10.1088/1748-9326/7/1/015201, 2012.
780 Semiletov, I.P., Shakhova, N.E., Pipko, I.I., Pugach, S.P., Charkin, A.N., Dudarev, O.V.,
781 Kosmach, D.A., and S. Nishino (2013). Space-time dynamics of carbon and

environmental parameters related to carbon dioxide emissions in the Buor-Khaya Bay of the Laptev Sea, Biogeosciences, 10, 5977-5996, doi:10.5194/bg-10-5977-2013

Semiletov I., Pipko I., Gustafsson O., Anderson L., Sergienko V., Pugach S., Dudarev O., Charkin A., Broder L., Andersson A., Spivak E., and N. Shakhova (2016), Acidification of the East Siberian Arctic Shelf waters through addition of freshwater and terrestrial carbon, Nature Geoscience, doi:10.1038/NEGO 2695, 2016.

Semiletov I.P., Pipko, I.I., Pivovarov, N.Y., Popov, V. V., Zimov, S. A., Voropaev, Y. V., and S.P. Davydov: Atmospheric carbon emissions from northern lakes: a factor of global significance, Atmospheric. Environment, 30, 1657-1671, 1996a.

Semiletov I.P., Pivovarov, N.Y., Pipko, I. I., Gukov, A. Y., Volkova, T. I., Sharp, J. P., Shcherbakov, Y. S., and K. P. Fedorov: Dynamics of dissolved CH_4 and CO_2 in the Lena River Delta and Laptev Sea. Transactions (Doklady) of the Russian Academy of Sciences, 350 (3), 401-404 (translated into English), 1996b.

Semiletov, I.P.: Destruction of the coastal permafrost ground as an important factor in biogeochemistry of the Arctic Shelf waters, Trans. (Doklady) Russian Acad. Sci., 368, 679-682 (translated into English), 1999.

Sessions, A.L., Burgoyne, T.W., and Hayes, J.M.: Determination of the H3 factor in hydrogen isotope ratio mass spectrometry, Anal. Chem. 73(2), 200-207, 2001.

Siewert, M.B., Hanisch, J., Weiss, N., Kuhry, P., Maximov, T.C., Hugelius, G.: Comparing carbon storage of Siberian tundra and taiga permafrost ecosystems at very high spatial resolution. J. Geophys. Res.: Biogeosciences, 120, doi:10.1002/2015JG002999, 2015.

Siewert, M.B., Hugelius, G., Heim, B., Faucherre, S.: Landscape controls and vertical variability of soil organic carbon storage in permafrost-affected soils of the Lena River Delta. Catena, 147, 725–741. doi:10.1016/j.catena.2016.07.048, 2016.

Soil Survey Staff: Keys to Soil Taxonomy, 12th ed., U.S. Department of Agriculture & Natural Resources Conservation Service, Washington, D. C., 2014.

Sessions, A. L., Burgoyne, T.W., Schimmelmann, A., and Hayes, J. M.: Fractionation of hydrogen isotopes in lipid biosynthesis, Org. Geochem., 30, 1193–1200, doi:10.1016/S0146-6380(99)00094-7, 1999.

Sessions, A.L., Sylva, S.P., Summons, R.E., and Hayers, J.M.: Isotopic exchange of carbon-bound hydrogen over geologic timescales, Geochim. Cosmochim. Ac. 68, 1545-1559, doi:10.1016/j.gca.2003.06.004, 2004.

Shakhova, N. and I. Semiletov: Methane release and coastal environment in the East Siberian Arctic shelf, Journal of Marine Systems, 66 (1-4), 227-243, 2007.

Shakhova, N., Semiletov, I., Leifer, I., , Sergienko, V., Salyuk, A., Kosmach, D., Chernikh D., Stubbs Ch., Nicolsky D., Tumskoy V., and O. Gustafsson: Ebullition and storm-induced methane release from the East Siberian Arctic Shelf, Nature Geoscience 7-1, 64-70, doi: 10.1038/NGEO2007, 2014.

Shakhova N., I. Semiletov, V. Sergienko, L. Lobkovsky, V. Yusupov, A. Salyuk, A. Salomatin, D. Chernykh, D. Kosmach, G. Panteleev, D. Nicolsky, V. Samarkin, S. Joye, A. Charkin, O. Dudarev, A. Meluzov, and Ö. Gustafsson: The East Siberian Arctic Shelf: towards further assessment of permafrost-related methane fluxes and

role of sea ice. Phil. Trans. R. Soc. A, vol. 373: 20140451. doi:10.1098/rsta.2014.0451, 2015.
Shanahan, T.M., Hughen, K.A., Ampel, L., Sauer, P.E., and Fornace, K.: Environmental controls on the 2H/1H values of terrestrial leaf waxes in the eastern Canadian Arctic, Geochim. Cosmochim. Ac. 119, 286-301, doi:10.1016/j.gca.2013.05.032, 2013.
Shiklomanov, N. I., Streletskiy, D. A., Little, J. D., and Nelson, F. E.: Isotropic thaw subsidence in undisturbed permafrost landscapes, Geophys. Res. Lett. 40, 6356-6361, doi:10.1002/2013GL058295, 2013.
Smith, F.A., and Freeman, K.H.: Influence of physiology and climate on dD of leaf wax n-alkanes from C3 and C4 grasses, Geochim. Cosmochim. Ac. 70, 1172-1187, doi:10.1016/j.gca.2005.11.006, 2006.
Strauss, J., Schirrmeister, L., Grosse, G., Wetterich, S., Ulrich, M., Herzschuh, U., and Hubberten, H.-W.: The deep permafrost carbon pool of the Yedoma region in Siberia and Alaska. Geophys. Res. Lett. 40, 6165-6170, doi:10.1002/2013GL058088, 2013.
Tesi, T., I. Semiletov, G. Hugelius, O. Dudarev, P. Kuhry, and Gustafsson, Ö.: Composition and fate of terrigenous organic matter along the Arctic land-ocean continuum in East Siberia: insights from biomarkers and carbon isotopes, Geochim. Cosmochim. Acta, 133, 235-256, 2014.
Tesi, T., Semiletov, I., Dudarev, O., Andersson, A., and Gustafsson, Ö.: Matrix association effects on hydrodynamic sorting and degradation of terrestrial organic matter during cross-shelf transport in the Laptev and East Siberian shelf seas, J. Geophys. Res.-Biogeosciences, 121, 731-752, doi:10.1002/2015JG003067, 2016a.
Tesi, T., Muschitiello, F., Smittenberg, R. H., Jakobsson, M., Vonk, J. E., Hill, P., Andersson, A., Kirchner, N., Noormets, R., Dudarev, O., Semiletov, I., and Gustafsson, Ö.: Massive remobilization of permafrost carbon during post-glacial warming, in review at Nature Communications, 2016b.
Vonk, J. E., van Dongen, B. E., and Gustafsson, Ö.: Selective preservation of old organic carbon fluvially released from sub-arctic soils, Geophys. Res. Lett. 37, L11605, 2010
Vonk, J. E., Sanchéz-García, L., van Dongen, B. E., Alling, V., Kosmach, D., Charkin, A., Semiletov, I. P., Dudarev, O. V., Shakhova, N., Roos, P., Eglinton, T. I., Andersson, A., and Gustafsson, Ö.: Activation of old carbon by erosion of coastal and subsea permafrost in Arctic Siberia, Nature, 489, 137–140, doi:10.1038/nature11392, 2012.
Vonk, J. E., and Gustafsson, Ö.: Permafrost-carbon complexities, Nat. Geosci. 6, 675-676, doi:10.1038/ngeo1937, 2013.
Vonk, J. E., Mann, P. J., Davydov, S., Davydova, A., Spencer, R. G. M., Schade, J., Sobczak, W. V., Zimov, N., Zimov, S., Bulygina, E., Eglinton, T. I., and Holmes, R. M.: High biolability of ancient permafrost carbon upon thaw, Geophys. Res. Lett., 40, 2689-2693, doi:10.1002/grl.50348, 2013.
Vonk, J. E., Semiletov, I. P., Dudarev, O. V., Eglinton, T. I., Andersson, A., Shakhova, N., Charkin, A., Heim, B., and Gustafsson, Ö.: Preferential burial of permafrost-derived organic carbon in Siberian-Arctic shelf waters, J. Geophys. Res. Oceans 119, 8410-8421, doi:10.1002/2014JC010261, 2014.

873 Vonk, J. E., Tank, S. E., Bowden, W. B., Laurion, I., Vincent, W. F., Alekseychik, P., Amyot,
874 M., Billet, M. F., Canario, J., Cory, R. M., Deshpande, B. N., Helbig, M., Jammet, M.,
875 Karlsson, J., Larouche, J., MacMillan, G., Rautio, M., Walter Anthony, K. M., and
876 Wickland, K. P.: Effects of permafrost thaw on Arctic aquatic ecosystems,
877 Biogeosciences 12, 7129-7167, doi:10.5194/bg-12-7129-2015, 2015.
878 Walvoord, M. A., Voss, C. I., and Wellman, T. P.: Influence of permafrost distribution
879 on groundwater flow in the context of climate-driven permafrost thaw: Example
880 from Yukon Flats Basin, Alaska, United States, Water Resour. Res. 48, W07524,
881 doi:10.1029/2011WR011595, 2012.
882 Weiss N, Blok D, Elberling B, Hugelius G, Jørgensen CJ, Siewert MB, Kuhry P:
883 Thermokarst dynamics and soil organic matter characteristics controlling initial
884 carbon release from permafrost soils in the Siberian Yedoma region. Sedimentary
885 Geology, http://dx.doi.org/10.1016/j.sedgeo.2015.12.004, 2015.
886 Wetterich, S., Tumskoy, V., Rudaya, N., Kuznetsov, V., Maksimov, F., Opel, T., Meyer,
887 H., Andreev, A. A., and Schirrmeister, L.: Ice Complex permafrost of MIS5 age in
888 the Dmitry Laptev Strait coastal region (East Siberian Arctic), Quaternary Science
889 Reviews, 147, 298-311, 10.1016/j.quascirev.2015.11.016, 2016.
890 Wiesenberg, G., Schwark, L., and Schmidt, M.: Improved automated extraction and
891 separation procedure for soil lipid analyses. European Journal of Soil Science 55,
892 349-356, 2014.
893 Wilkie, K.M.K., Chapligin, B., Meyer, H., Burns, S., Petsch, S., and Brigham-Grette, J.:
894 Modern isotope hydrology and controls on dD of plant leaf waxes at Lake
895 El'gygytgyn, NE Russia, Clim. Past 9, 335-352, doi:10.5194/cp-9-335-2013, 2013.
896 Winterfeld, M., Lepple, T., and Mollenhauer, G.: Characterization of particulate
897 organic matter in the Lena River delta and adjacent nearshore zone, NE Siberia –
898 Part I: Radiocarbon inventories, Biogeosciences, 12, 3769-3788, doi:10.5194/bg-
899 12-3769-2015, 2015.
900 Yang, H., Liu, W., Leng, Q., Hren, M.T., and Pagani, M.: Variation in n-alkane dD values
901 from terrestrial plants at high latitude: implications for paleoclimate
902 reconstruction, Org. Geochem. 42, 283-288,
903 doi:10.1016/j.orggeochem.2011.01.006, 2011.
904 Zech, R., Huang, Y., Zech, M., Tarozo, R., and W. Zech: High carbon sequestration in
905 Siberian permafrost loess-paleosols during glacials, Clim. Past, 7, 501-509,
906 doi:10.5194/cp-7-501-2011, 2011.
907 Zimov, S.A., Semiletov, I. P. Daviodov, S. P., Voropaev, Y. V., Prosyannikov, S. F., Wong,
908 C. S., and Y.-H. Chan: Wintertime CO_2 emission from soils of Northeastern Siberia.
909 Arctic, 46, 197-204, 1993.
910

Figure 1
Map of coastal northeast Siberia showing the extent of ice complex permafrost (ICD; red) overlaid with the location of ice complex (n=9; black diamonds) and topsoil samples (n=9; green squares). The shelf-slope Laptev Sea transect is shown with yellow stars.

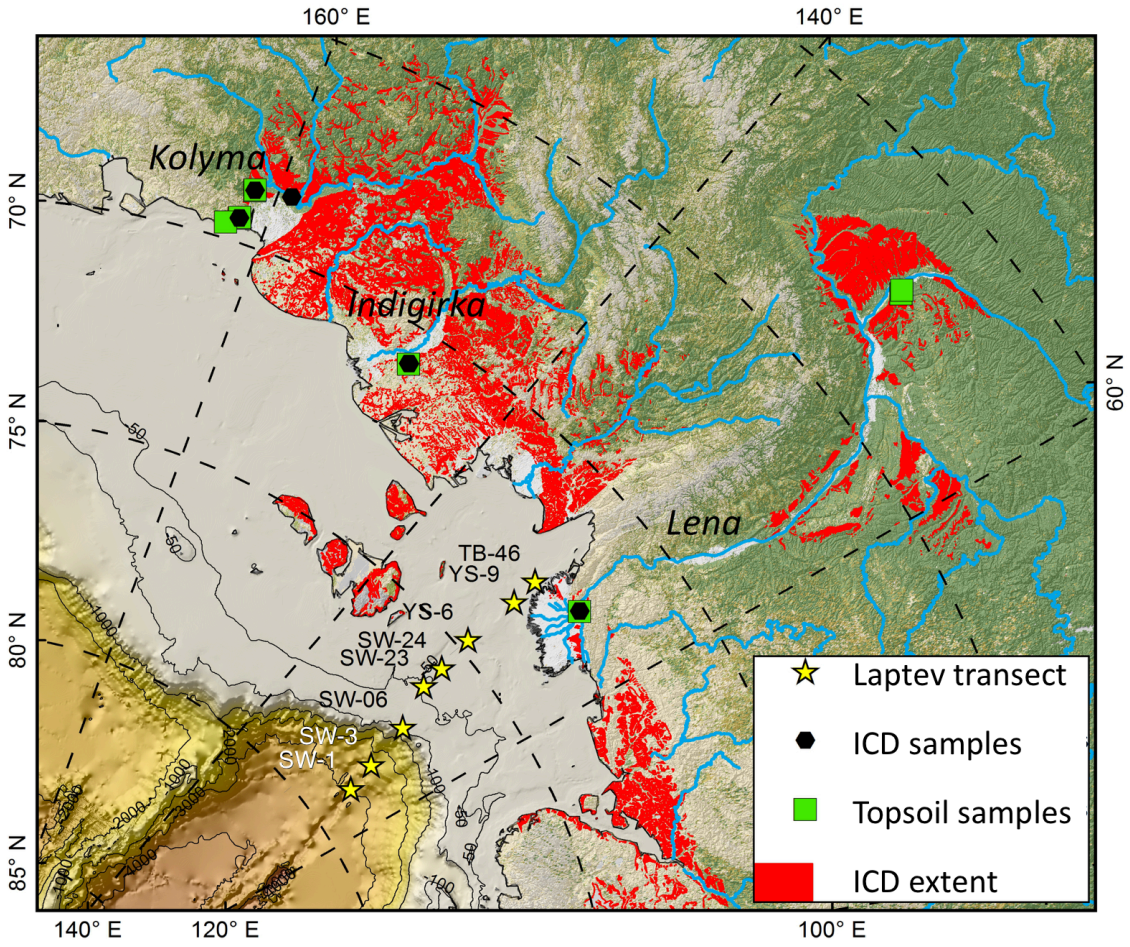

Figure 2

Molecular concentrations and ratios of topsoil Holocene permafrost (green; n=9) and deeper Pleistocene permafrost (blue; n=9) samples, with (a) the sum of odd *n*-alkanes C_{25}-C_{31}, (b) the sum of even *n*-alkanoic acids C_{22}-C_{28}, (C) the Carbon Preference Index (CPI) for *n*-alkanes C_{23}-C_{31}, (d), the CPI for *n*-alkanoic acids C_{22}-C_{28}, (e) the ratio of C_{23} over $C_{23}+C_{29}$ *n*-alkanes, and (f) the sum of high-molecular weight (HMW) *n*-alkanoic acids over HMW *n*-alkanes. The CPI is calculated as $CPI_{i\text{-}n} = ½ \Sigma (X_i+X_{i+2}+...+X_n)/ \Sigma (X_{i-1}+X_{i+1}+...+X_{n-1}) + ½ \Sigma (X_i+X_{i+2}+...+X_n)/ \Sigma (X_{i+1}+X_{i+3}+...+X_{n+1})$, where X is concentration. Stars indicate that the two compared values are statistically significant (95% confidence). Note that panel a and b are reported as median with IQR (interquartile range) and the other panels are reported as average±standard deviation.

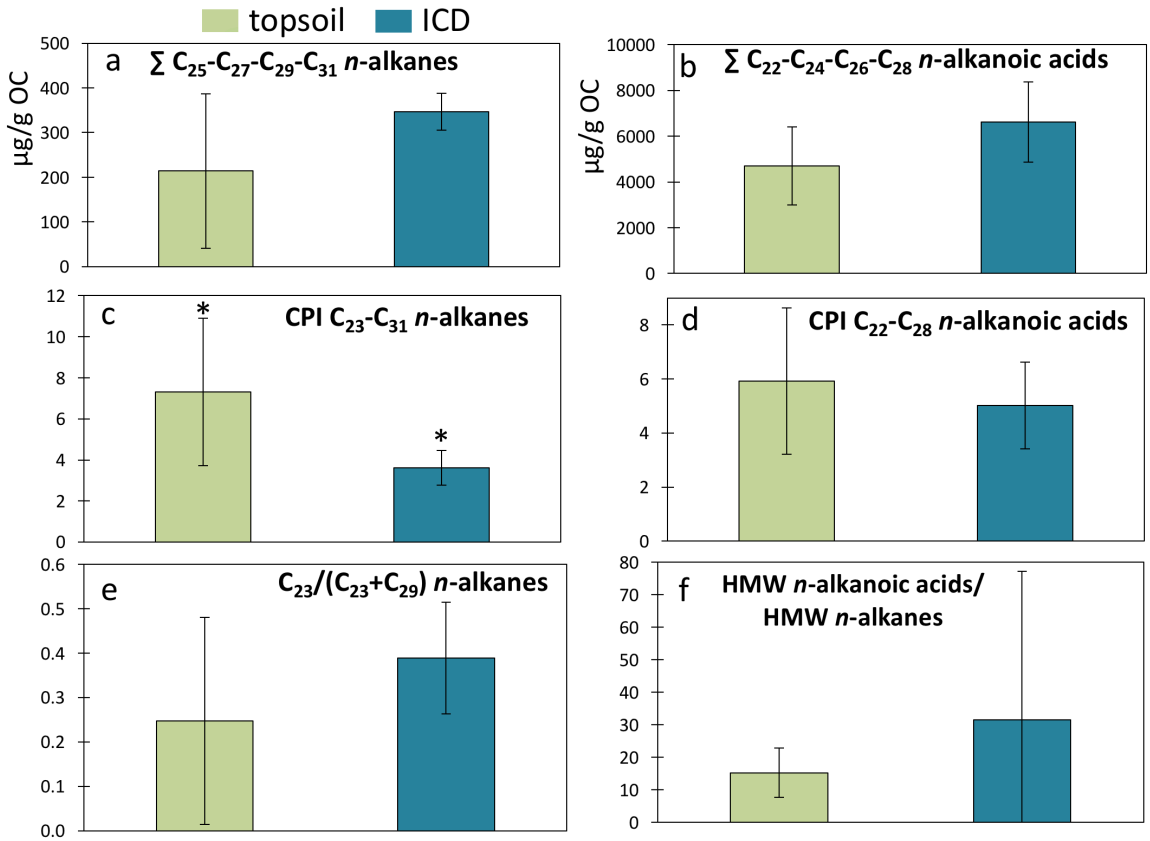

Figure 3

Molecular isotopic signature against chain length of long chain *n*-alkanoic acids (top) and *n*-alkanes (bottom) for Holocene topsoil samples (green) and Pleistocene ice complex samples (ICD; blue). Stars indicate that the two compared values are statistically significant (95% confidence). Standard deviations are represented as vertical bars, and are smaller than the sample circles when not visible.

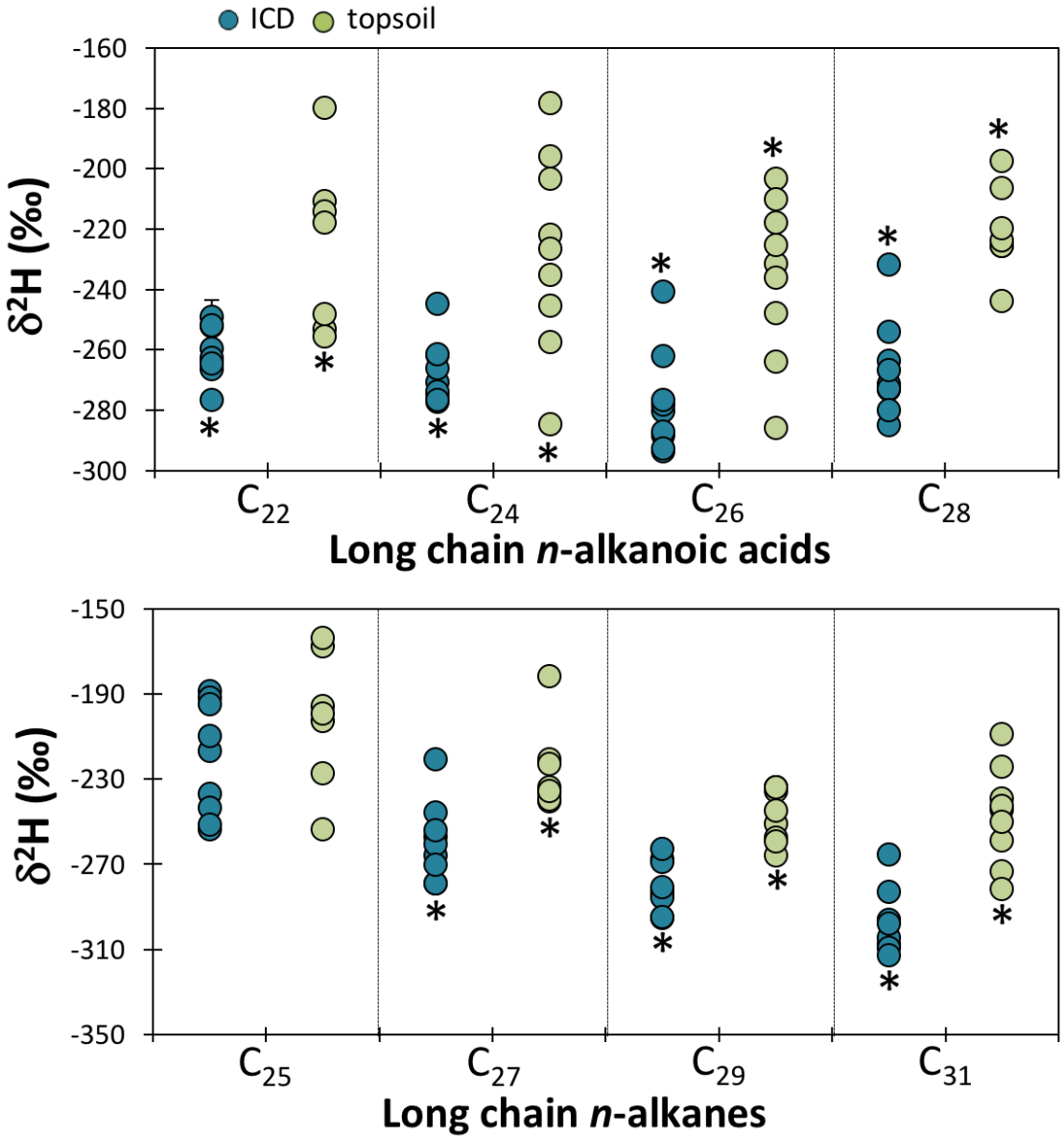

Figure 4

Concentration-weighted mean δ^2H values of C_{27}-C_{29}-C_{31} *n*-alkanes plotted against concentration-weighted mean δ^2H values of C_{24}-C_{26}-C_{28} *n*-alkanoic acids to illustrate the fractionation differences between these two leaf wax markers. Dashed line indicates an identical fractionation.

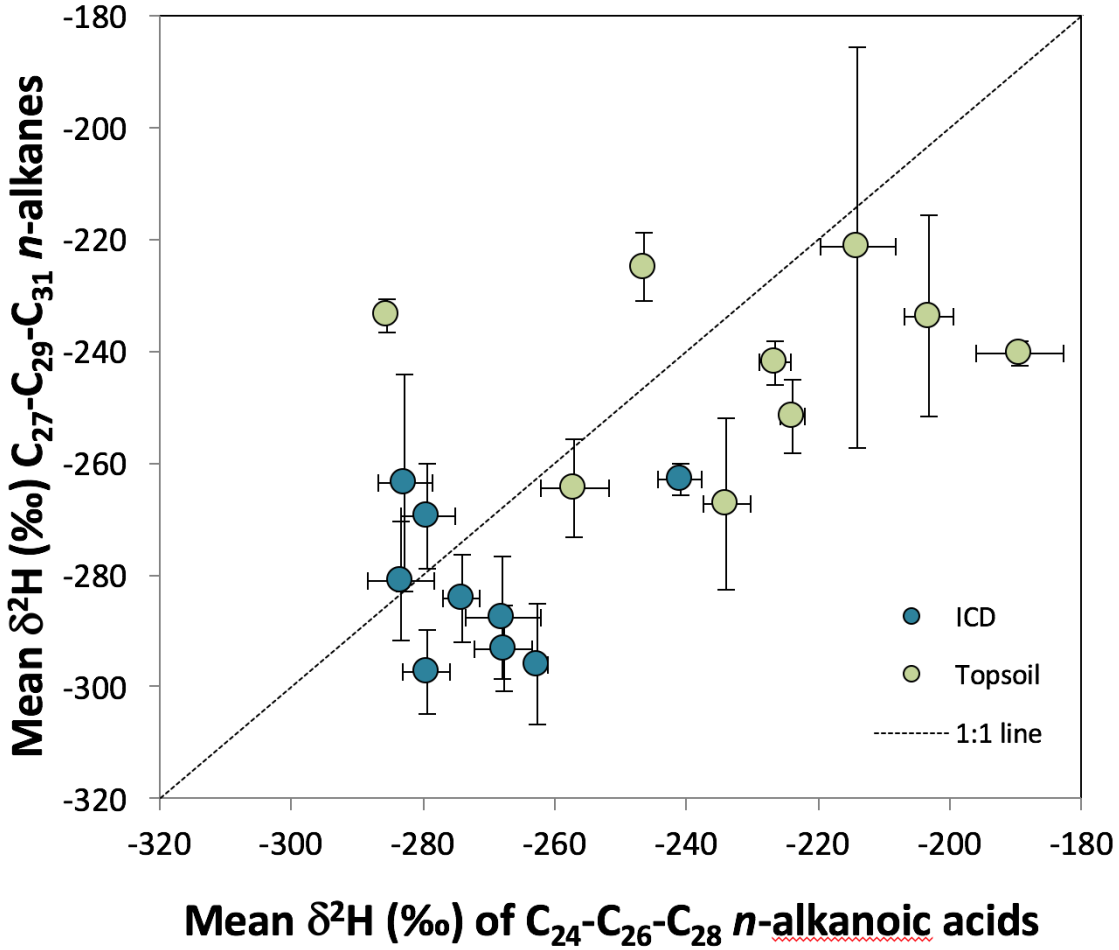

Figure 5

Comparison of δ^2H values of C_{28} *n*-alkanoic acid (left) and C_{29} *n*-alkane (right) in modern (Topsoil-PF; green circles) and ICD-PF for this study (blue circles) and available literature, with crosses from Zech et al. (2011; glacial and interglacial paleosoils from permafrost bluff exposure at Tumara River northeast Siberia), black triangles from Yang et al. (2011; C3 plants and trees from Canada and Alaska), light grey triangles from Wilkie et al. (2013; C3 plants from the El'gygytgyn lake basin, Siberia), white triangles from Pautler et al. (2014; modern and paleosoils from the Yukon territory, Canada) and dark grey triangles from Porter et al. (2016; muck deposits from the Yukon territory, Canada).

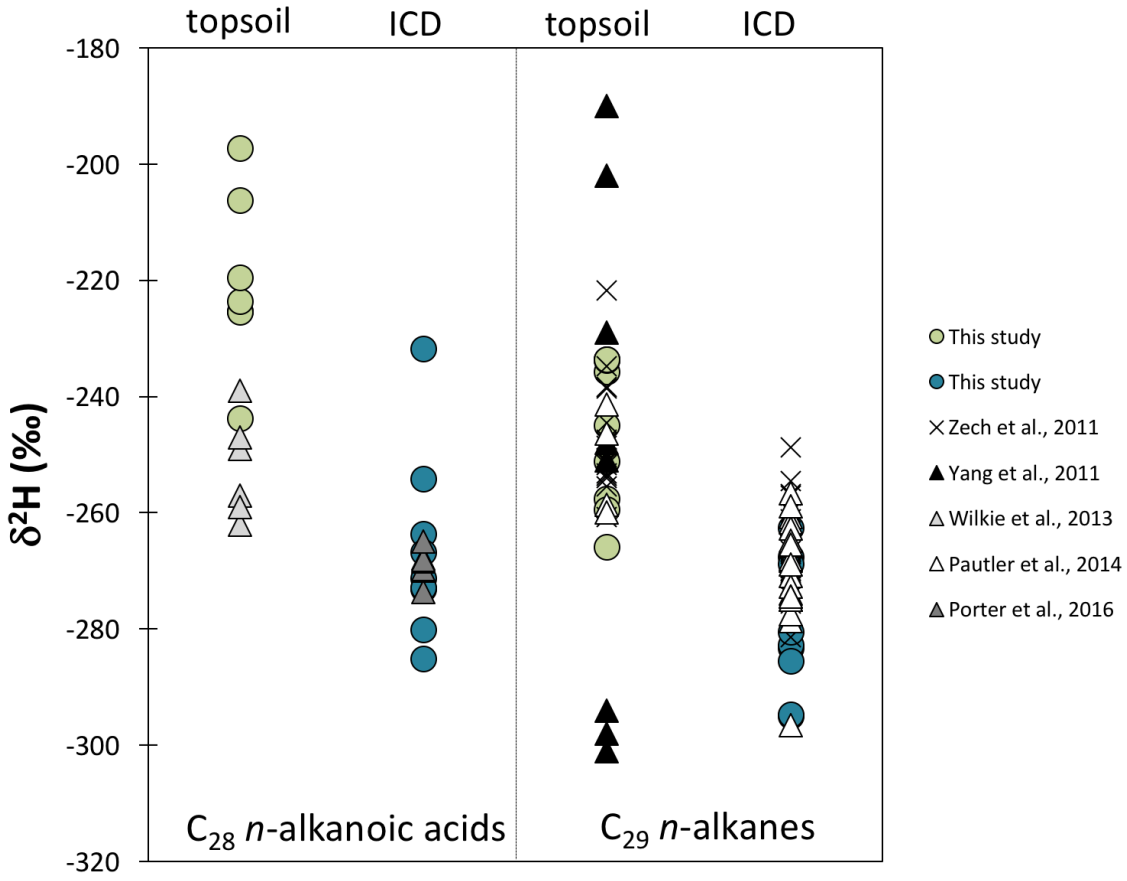

Figure 6

Contribution of OC from Topsoil-PF (green) and ICD-PF (blue) sources to surface sediments along a shelf-slope transect in the Laptev Sea (see also Bröder et al., 2016b for further transect information), calculated with a $\delta^{13}C$- $\Delta^{14}C$ (triangles) and leaf wax $\delta^{2}H$ mixing model (circles). Stations are plotted against log water depth (m; see also Table 6) following the transect order from the coastal, nearshore, zone in the South (furthest left; TB-46, 6 m depth) towards the continental rise in the North (furthest right; SW-01, 3146 m depth). Topsoil $\Delta^{14}C$ end-member values are corrected for cross-shelf transport time (see section 4.2).

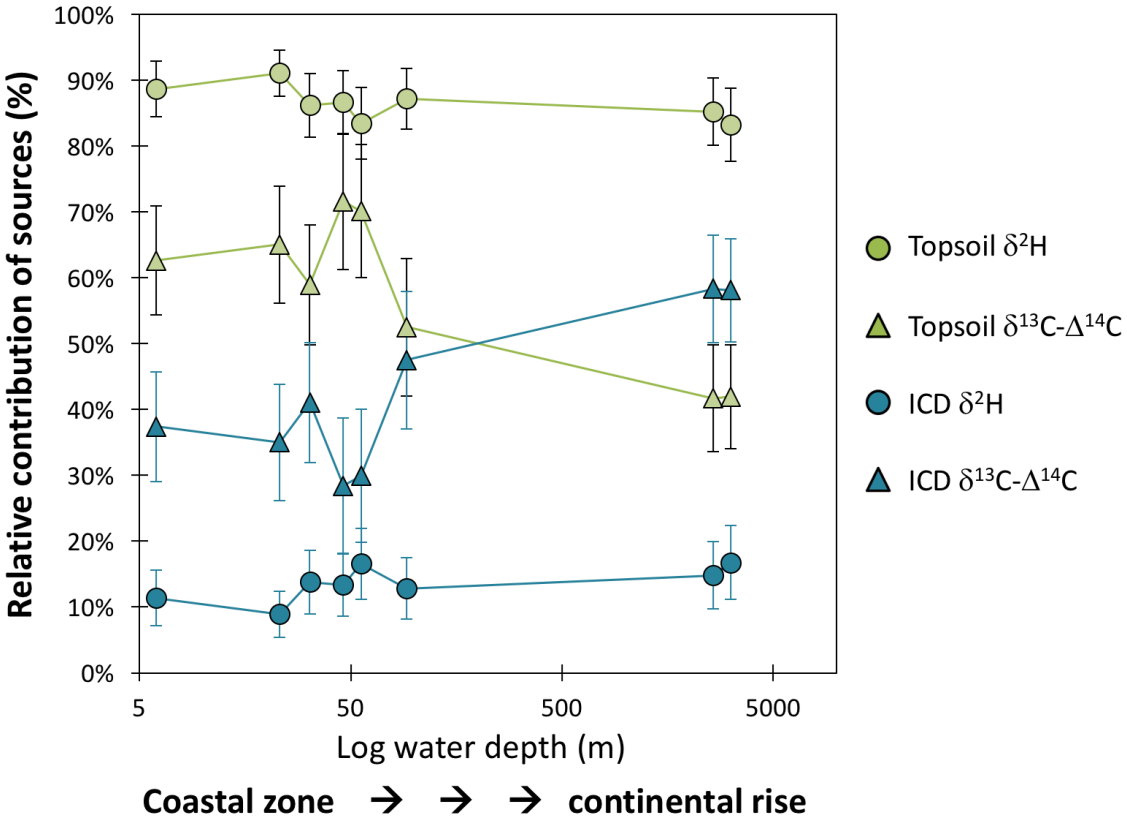

Table 1
Site characteristics and geochemical properties of eight topsoil and eight ice complex deposit samples. A table with more detailed sample descriptions can be found in Supplementary Table 1.

Sample code	Sample ID	Current vegetation	Watershed	Description	Lat	Lon	TOC	$\delta^{13}C$	^{14}C-yrs	TN	C/N
					°N	°E	%	‰		%	
Topsoil (modern vegetation and O-horizon samples)											
TS-1	KU EXP 1-1, 0-16 cm	Tundra	Lena	Surface O-horizon; 0-16 cm	72.34	126.29	11	-27.0	n.a.	0.40	27.5
TS-2	CH YED2, 0-4 cm	Tundra	Kolyma	Surface O-A horizon; 0-4 cm	69.46	161.79	17	-28.4	n.a.	0.64	26.5
TS-3	SP T3-3B,	Alas grassland	Lena	Alas soil (Mollisol), mix of O and A horizon	62.32	129.50	15	-27.9	n.a.	1.40	10.7
TS-4	SP T2-7,	Larch taiga	Lena	Taiga soil (turbel), mix of O and A horizon	62.25	129.62	13	-28.4	n.a.	0.45	28.0
TS-5	KY T2-3,	Tussock tundra	Indigirka	Tundra soil (turbel), O-horizon	70.83	147.48	29	-28.5	n.a.	1.56	18.7
TS-6	CH T2-1,	Tussock tundra	Kolyma	Tundra soil (turbel), mix of O, Ojj and Ajj horizons	69.44	161.77	21	-26.4	n.a.	0.57	36.7
TS-7	CH YED3, 0-10 cm	Larch taiga	Kolyma	Surface O-hor; 0-10 cm	68.77	161.41	39	-29.6	n.a.	1.29	30.7
TS-8G[a]	CH Medv grass[a]	Grass tundra	Kolyma	Vegetation	69.64	162.54	41	-25.2	n.a.	1.47	27.8
TS-9G[a]	CH Y4 grass[a]	Larch taiga	Kolyma	Vegetation	68.74	161.41	40	-28.5	n.a.	2.42	16.6
	Mean values						**25**	**-27.8**		**1.1**	**24.8**
	Ice complex deposits										
ICD-1	KU EXP 1-3, 212-216 cm	Tundra	Lena	Very deep undisturbed yedoma ca. 10 m below surface	72.34	126.29	1.3	-27.5	n.a.	0.08	15.7
ICD-2	CH YED1, 300-305 cm	Tussock tundra	Kolyma	Deep undisturbed yedoma ca. 3 m below surface	69.47	161.77	1.4	-26.3	n.a.	0.14	10.2
ICD-3	CH YED2, 300-305 cm	Tussock tundra	Kolyma	Deep undisturbed yedoma ca. 3 m below surface	69.46	161.79	2.3	-25.8	n.a.	0.27	8.6
ICD-4	CH YED3, 520-525 cm	Larch taiga	Kolyma	Deep undisturbed yedoma ca. 5 m below surface	68.77	161.41	1.4	-25.5	n.a.	0.15	9.7
ICD-5	KY EXP1, 0-5 cm	Tussock tundra	Indigirka	Undisturbed yedoma ca. 2 m below surface	70.83	147.44	1.5	-25.5	27920 ±210	0.18	8.5

ICD-6	KY EXP2, 110-115 cm	Tussock tundra	Indigirka	Deep undisturbed yedoma ca. 4.5 m below surface	70.83	147.44	1.6	-25.6	17270 ±80	0.19	8.6
ICD-7	KY EXP3, 185-190 cm	Tussock tundra	Indigirka	Undisturbed yedoma ca. 2 m below surface	70.83	147.49	1.5	-25.2	n.a.	0.17	8.5
ICD-8	CH DY-3A	Larch taiga	Kolyma	Particulate matter from thaw streams	68.63	159.15	1.5[b]	-25.2[b]	19370 ±70	-	-
ICD-9	CH DY-4A	Larch taiga	Kolyma	Particulate matter from thaw streams	68.63	159.15	1.4[b]	-25.1[b]	28040 ±140	-	-
	Mean values						**1.6**	**-25.7**		**0.2**	**10.0**

a vegetation/grass samples, labelled with "G"
b data from Vonk et al., 2013

Table 2
Long-chain *n*-alkane concentrations (in µg/gOC) of topsoil Holocene samples (modern vegetation/O-horizon) and Pleistocene ice complex samples.

	C21	C22	C23	C24	C25	C26	C27	C28	C29	C30	C31	C32	C33
	µg/g OC												
Topsoil (modern vegetation and O-horizon samples)													
TS-1	44	88	96	45	41	10	45	4.4	27	2.5	36	1.5	7.2
TS-2	24	15	21	12	40	10	160	10	150	6.5	150	3.5	17
TS-3	2.5	2.4	5.9	2.6	13	4.7	42	16	74	4.7	85	2.7	24
TS-4	19	3.3	7.1	2.7	27	4.5	47	6.7	98	9.1	150	5.7	38
TS-5	35	8.4	26	9.9	38	13	91	18	180	14	230	8.1	43
TS-6	14	5.1	16	5.7	19	4.0	26	3.7	48	5.0	120	4.0	32
TS-7	46	12	18	8.8	22	16	61	27	220	23	340	12	48
TS-8G	4.1	1.7	18	10	61	16	47	13	30	5.3	10	1.1	1.1
TS-9G	4.7	2.6	18	15	45	21	50	16	31	6.8	9.8	1.5	2.6
Ice complex deposits													
ICD-1	57	79	100	49	82	23	170	16	137	8.5	140	4.4	25
ICD-2	55	89	100	70	70	27	75	20	130	12	120	5.3	28
ICD-3	40	64	74	31	54	15	79	22	110	10	160	4.8	32
ICD-4	60	93	98	47	55	20	84	22	140	12	150	6.0	39
ICD-5	46	79	86	56	49	20	55	13	75	7.0	100	4.7	38
ICD-6	41	73	87	68	62	29	65	20	98	11	120	4.9	27
ICD-7	50	83	83	43	41	16	65	17	100	8.3	120	4.5	42
ICD-8	4.2	7.3	23	30	55	42	82	38	100	18	110	5.0	21
ICD-9	6.2	6.2	16	11	29	15	51	20	79	9.3	85	4.1	23

Table 3
Long-chain *n*-alkanoic acids concentrations (in µg/gOC) of topsoil Holocene samples (modern vegetation/O-horizon) and Pleistocene ice complex samples.

	C16	C18	C20	C21	C22	C23	C24	C25	C26	C27	C28	C29	C30
	µg/gOC												
Topsoil (modern vegetation and O-horizon samples)													
TS-1	511	220	176	80.5	539	311	1100	4.95	684	90.5	350	32.8	58.1
TS-2	1740	664	673	235	1380	496	1390	543	1740	409	1580	113	305
TS-3	664	296	480	116	1020	504	1710	415	1550	250	1060	132	456
TS-4	1140	408	665	235	1400	431	1410	425	1250	242	651	143	455
TS-5	513	343	530	133	1140	359	1410	1.58	896	119	494	67.8	224
TS-6	1080	537	418	236	1420	790	2670	2.82	1570	127	657	46.6	174
TS-7	1420	352	538	281	1850	722	2010	651	1790	642	1580	730	1971
TS-8G	3640	855	691	44.1	609	63.5	156	26.0	224	0.122	99.3	9.91	28.1
TS-9G	4600	887	966	53.6	815	66.7	261	28.6	232	11.5	124	8.10	30.2
Ice complex deposits													
ICD-1	1750	1600	4560	1460	9460	2300	8930	2020	5830	1030	3660	293	635
ICD-2	10400	4030	5800	2410	17100	7270	18600	6610	16600	5860	14800	6810	18700
ICD-3	665	554	892	263	2070	1060	3070	646	2340	272	1310	133	532
ICD-4	1400	769	1030	252	2040	910	3120	644	2440	266	1160	124	432
ICD-5	426	304	447	126	1220	511	1970	70.4	1390	133	712	60.7	233
ICD-6	722	539	583	153	1370	606	2270	457	1970	181	1030	86.4	333
ICD-7	446	313	543	158	1330	562	2350	401	1370	154	743	63.1	230
ICD-8	920	402	895	108	1070	294	1180	184	799	70.3	331	34.4	100
ICD-9	327	200	559	74	803	229	1010	2.17	718	64.9	334	28.7	104

Table 4

Sum of most abundant long-chain *n*-alkanoic acids and *n*-alkanes (concentrations in µg/gOC), and characteristic ratios of *n*-alkanoic acids and *n*-alkanes of topsoil Holocene (modern vegetation/O-horizon) and Pleistocene ice complex samples.

	***n*-alkanoic acids**				***n*-alkanes**				
	ΣHMW[a] (>C_{22}) *µg/gOC*	**ΣC_{22}-C_{28} (even)** *µg/gOC*	**CPI[b]**	**HMW acids/ HMW alkanes[a]**	**ΣHMW[a] (>C_{21})** *µg/gOC*	**ΣC_{25}-C_{31} (odd)** *µg/gOC*	**CPI[c]**	**C_{23}/ (C_{23}+C_{23})**	**C_{25}/ (C_{25}+C_{29})**
Topsoil (modern vegetation and O-horizon samples)									
TS-1	3167	2670	5.8	7.1	447	148	2.7	0.78	0.60
TS-2	7958	6090	3.8	13	612	494	11	0.12	0.21
TS-3	7095	5340	4.1	25	280	214	7.2	0.07	0.15
TS-4	6397	4700	3.7	15	418	323	12	0.07	0.21
TS-5	4715	3940	6.8	6.6	717	543	9.1	0.12	0.17
TS-6	7454	6310	6.0	25	300	211	9.9	0.25	0.28
TS-7	11950	7230	2.9	14	857	647	7.8	0.08	0.09
TS-8G	1216	1090	9.5	5.6	217	148	3.7	0.37	0.67
TS-9G	1577	1430	11	7.1	223	135	2.5	0.36	0.59
Mean±stdev	*5726±3431*	*4310±2190*	*5.9*	*13*	*452±230*	*318±195*	*7.3*	*0.25*	*0.33*
Median and IQR	6397^{7454}_{3167}	4700^{2670}_{6092}	*2.7*	*7.6*	418^{621}_{280}	214^{494}_{148}	*3.6*	*0.23*	*0.22*
Ice complex deposits									
ICD-1	34854	27883	4.1	39	893	530	4.9	0.43	0.38
ICD-2	112356	67078	2.8	140	806	398	3.0	0.44	0.35
ICD-3	11430	8791	4.1	16	698	405	4.6	0.40	0.33
ICD-4	11145	8768	4.4	14	825	428	3.8	0.42	0.29
ICD-5	6293	5285	6.5	10	630	280	2.9	0.54	0.40
ICD-6	8293	6629	4.9	12	708	347	2.7	0.47	0.39
ICD-7	7196	5787	4.7	11	671	323	3.5	0.45	0.29
ICD-8	4063	3380	5.5	7.6	533	344	2.7	0.19	0.35
ICD-9	3295	2867	8.3	9.3	355	244	4.3	0.17	0.27
Mean±stdev	*22103±35150*	*15160±20800*	*5.0*	*29*	*680±163*	*367±85*	*3.6*	*0.39*	*0.34*
Median and IQR	8290^{11430}_{6290}	6630^{8790}_{5285}	*1.6*	*43*	698^{806}_{630}	347^{405}_{323}	*0.8*	*0.13*	*0.05*

a HMW; high-molecular weight

b CPI; carbon preference index for chain lengths C_{22}-C_{28}, for calculation see caption of Fig. 2.

c CPI; carbon preference index for chain lengths C_{23}-C_{31}, for calculation see caption of Fig. 2.

Table 5

δ^2H signatures (in ‰) of *n*-alkanoic acids and *n*-alkanes of topsoil Holocene (modern vegetation/O-horizon) and Pleistocene ice complex samples.

	***n*-alkanoic acids**							***n*-alkanes**			
	C16	**C18**	**C20**	**C22**	**C24**	**C26**	**C28**	**C25**	**C27**	**C29**	**C31**
Topsoil (modern vegetation and O-horizon samples)											
TS-1	-162	-180		-119	-178	-203	-197	-168	-240	-236	-244
TS-2	-188	-192		-211	-222	-232	-225	-196	-237	-251	-239
TS-3				-126	-203	-218	-225		-125	-234	-259
TS-4	-171	-213		-180	-196	-210	-206		-182	-245	-243
TS-5		-235	-185	-253	-257	-264	-244	-164	-240	-266	-273
TS-6	-189	-222		-214	-235	-236	-224	-203	-221	-258	-282
TS-7	-184		-190	-218	-227	-225	-220	-199	-234	-259	-250
TS-8G	-258	-246	-253	-256	-285	-286		-253	-236	-234	-224
TS-9G	-237	-244	-251	-248	-245	-248		-227	-223	-234	-209
Mean	*-199*	*-219*	*-220*	*-203*	*-228*	*-236*	*-220*	*-201*	*-215*	*-246*	*-247*
St.dev	35	25	37	52	33	27	15	*32*	*39*	*13*	*23*
Ice complex deposits											
ICD-1	-194	-227	-243	-252	-245	-241	-232	-237	-257	-268	-265
ICD-2			-231	-264	-271	-280	-271	-217	-266	-283	-297
ICD-3				-249	-262	-278	-264	-254	-279	-283	-307
ICD-4			-209	-252	-266	-277	-254	-243	-261	-285	-305
ICD-5			-169	-260	-275	-288	-273	-189	-245	-269	-283
ICD-6	-211	-216	-252	-266	-274	-294	-285	-192	-254	-281	-296
ICD-7			-191	-263	-277	-287	-273	-210	-279	-295	-309
ICD-8	-244	-256	-277	-277	-277	-293	-280	-195	-221	-263	-298
ICD-9	-228	-229	-261	-265	-262	-262	-267	-251	-270	-295	-313
Mean	*-219*	*-232*	*-229*	*-261*	*-268*	*-278*	*-267*	*-221*	*-259*	*-280*	*-297*
St.dev	21	17	37	8.6	10	17	16	*26*	*18*	*12*	*15*

Table 6

Location, sampling depth and isotopic values of samples along a surface sediment transect in the Laptev Sea (data from Bröder et al., 2016b), with percentage topsoil (TS) and ice complex deposit (ICD) OC contributions to the samples based on source-apportionment calculations with δ^2H leaf wax end-members versus $\delta^{13}C$-$\Delta^{14}C$ end-members (end-member values are described in the text).

				Sample values						**Source contributions**			
ID[a]	**Lat**	**Long**	**Depth**	**C_{27}**	**C_{29}**	**C_{31}**	**$C_{27\text{-}29\text{-}31}$**[b]	**$\delta^{13}C$**	**$\Delta^{14}C$**	**TS**	**ICD**	**TS**[c]	**ICD**[c]
	N	°E	m	‰	‰	‰	‰	‰	‰	using δ^2H		using $\delta^{13}C$-$\Delta^{14}C$	
TB-46	72.700	130.180	6	-236.2	-237.4	-230.4	-235.0	-26.5	-436	89%	11%	63% (63%)	37% (37%)
YS-9	73.366	129.997	23	-233.7	-231.0	-227.8	-231.1	-26.1	-415	91%	8.9%	63% (65%)	37% (35%)
YS-6	74.724	130.016	32	-234.2	-241.0	-235.4	-236.8	-25.6	-465	86%	14%	51% (59%)	49% (41%)
SW-24	75.599	129.558	46	-229.3	-236.5	-243.5	-236.4	-24.8	-284	87%	13%	70% (72%)	30% (28%)
SW-23	76.171	129.333	56	-219.9	-243.3	-243.3	-236.0	-25.0	-333	83%	17%	65% (70%)	35% (30%)
SW-06	77.142	127.378	92	-219.5	-237.0	-241.4	-233.2	-23.2	-364	87%	13%	39% (53%)	61% (47%)
SW-03	78.238	126.150	2601	-221.1	-238.0	-247.7	-235.9	-22.6	-426	85%	15%	23% (42%)	77% (58%)
SW-01	78.942	125.243	3146	-223.8	-241.8	-246.0	-238.0	-22.3	-418	83%	17%	21% (42%)	79% (58%)

a Location, depth and bulk carbon isotope data from Bröder et al. (2016b)

b weighted average based on individual concentrations

c numbers in brackets are source contributions using the $\delta^{13}C$-$\Delta^{14}C$ approach but with additional corrections for cross-shelf lateral transport time of topsoil OC (similar as in Bröder et al., 2016a); we applied linear aging along the transect based on the distance from the coast, with a maximum aging of 5000 years for station SW-01.